CAL-2140

National Aeronautics and Space Administration

COMBINED ANNUAL STATUS REPORT & FINAL TECHNICAL REPORT FOR NAG 5-2051

29P

Prepared by:

Columbia Astrophysics Laboratory
Departments of Astronomy and Physics
Columbia University
538 West 120^{th} Street
New York, New York 10027

Submitted by:

The Trustees of Columbia University
in the City of New York
Box 20, Low Memorial Library
New York, NY 10027

Title of Research: Multiwavelength Observations of Unidentified High Energy Gamma-Ray Sources

Principal Investigator:

Jules P. Halpern
Columbia University

Period Covered by Report: 15 August 1992 – 14 October 1993

October 1993

Multiwavelength Observations of Unidentified High-Energy Gamma-Ray Sources

Combined Annual Status Report and Final Technical Report

Summary

As was the case for *COS B*, the majority of high-energy (> 100 MeV) γ-ray sources detected by the EGRET instrument on GRO are not immediately identifiable with catalogued objects at other wavelengths. These persistent γ-ray sources are, next to the γ-ray bursts, the least understood objects in the universe. Even a rudimentary understanding of their nature awaits identifications and follow-up work at other wavelengths to tell us what they are. The as yet unidentified sources are potentially the most interesting, since they may represent unrecognized new classes of astronomical objects, such as radio-quiet pulsars or new types of AGNs.

This two-year investigation is intended to support the analysis, correlation, and theoretical interpretation of data that we are obtaining at X-ray, optical, and radio wavelengths in order to render the γ-ray data interpretable. According to plan, in the first year we concentrated on the identification and study of Geminga. The second year will be devoted to studies of similar unidentified γ-ray sources which will become available in the first EGRET catalogs.

The results obtained so far are presented in the two papers which are reproduced in the Appendix. In these papers, we discuss the pulse profiles of Geminga, the geometry and efficiency of the magnetospheric accelerator, the distance to Geminga, the implications for theories of polar cap heating, the effect of the magnetic field on the surface emission and environment of the neutron star, and possible interpretations of a radio-quiet Geminga. We also discuss the implications of the other γ-ray pulsars which have been discovered to have high γ-ray efficiency, and attribute the remaining unidentified *COS B* sources to a population of efficient γ-ray sources, some of which may be radio quiet.

APPENDIX

Papers Published Under NASA Grant NAG 5-2051

"Soft X-ray Properties of the Geminga Pulsar," J. P. Halpern & M. Ruderman, *Ap. J.*, **415**, 286–297 (1992).

"Gamma-ray Pulsars and Geminga," M. Ruderman, K. Chen, K. S. Cheng, & J. P. Halpern, in *Compton Gamma-Ray Observatory*, eds. M. Friedlander, N. Gehrels, & D. J. Macomb (New York: AIP), pp. 259–271 (1993).

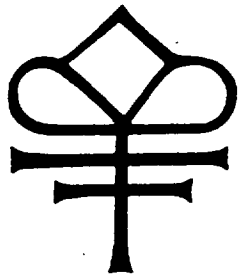

GAMMA-RAY PULSARS AND GEMINGA

M. Ruderman
Department of Physics & Columbia Astrophysics Laboratory
Columbia University

K. Chen
Los Alamos National Laboratory

K.S. Cheng
Department of Physics, University of Hong Kong

and

J.P. Halpern
Department of Astronomy & Columbia Astrophysics Laboratory
Columbia University

COLUMBIA UNIVERSITY

DEPARTMENTS OF

PHYSICS and ASTRONOMY

NEW YORK, NEW YORK 10027

Columbia Astrophysics Laboratory Contribution Number 510

GAMMA-RAY PULSARS AND GEMINGA

M. Ruderman
Department of Physics & Columbia Astrophysics Laboratory
Columbia University

K. Chen
Los Alamos National Laboratory

K.S. Cheng
Department of Physics, University of Hong Kong

and

J.P. Halpern
Department of Astronomy & Columbia Astrophysics Laboratory
Columbia University

ABSTRACT

Observed properties of γ-ray pulsars are related to those of the accelerators which power their radiation. It is argued that the relatively slowly spinning Geminga is a strong γ-ray source only because its magnetic dipole is more inclined than that of the more rapidly spinning Vela. This would also account for special Geminga properties including 180° subpulse separation, soft X-ray spectra and intensities, and suppression of radio emission.

1. INTRODUCTION

A number of common properties suggest that the family of strongly emitting γ-ray pulsars are all powered by similar accelerators. In most, and perhaps all of these pulsars, the "light curve" for emission of γ-rays consists of two subpulses. The EGRET γ-ray pulse profile for the Vela radiopulsar is shown in Fig. 1. The phase separation for it and others in this family ($\Delta\phi$ on a scale of 0 to 1) are shown in Table 1.

Although spectral breaks seem to occur at various energies below 10^2 MeV, above that energy the γ-ray flux per unit energy (E) varies as E^{-2} up to energies well above a GeV.

Some total γ-ray luminosities (for an assumed fan beam geometry) are indicated in Fig. 2. Although these absolute luminosities (L_γ) seem to decrease with increasing period (P), the ratio of γ-ray power to the total stellar spin-down power ($I\Omega\dot{\Omega}$) seems to increase. A probable Geminga distance, 250 ± 150 pc[1], somewhat less than that to the Vela pulsar, suggests that its L_γ is comparable to that of the Vela pulsar

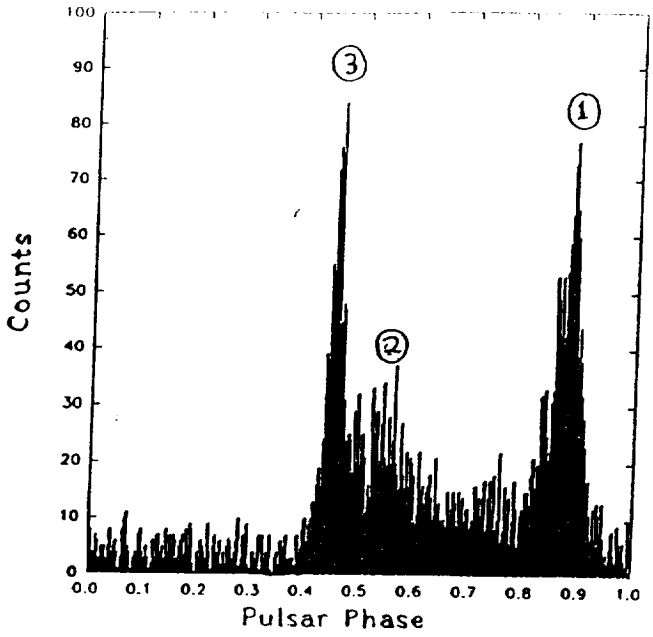

Fig. 1. The γ-ray light curve of the Vela radiopulsar as observed by EGRET[2] during Aug. – Sept. 1991. The photon energies > 50 MeV.

Table 1. Subpulse Separation in γ-ray Pulsars

Pulsar	Period (s)	$\Delta\phi$
Crab	0.033	0.4
PSR 0540 – 69[a]	0.050	0.2
Vela	0.089	0.4
PSR 1706 – 44	0.102	≤ 0.2 ?
Geminga	0.237	0.5

[a]PSR 0540 – 69 appears to be extremely similar to the Crab pulsar in almost every way but it is so distant that it has not yet been confirmed as a γ-ray source. The broad PSR 1706 – 44 γ-ray pulse has not been resolved.

despite a neutron star spin-down power which is two orders of magnitude less.

These γ-ray pulsar family similarities support the hypothesis that the γ-ray emission may be understood as a consequence of a common accelerator which differs among these pulsars because of their different ($\vec{\Omega}$), angle between $\vec{\Omega}$ and the stellar magnetic dipole moment $\vec{\mu}$, and

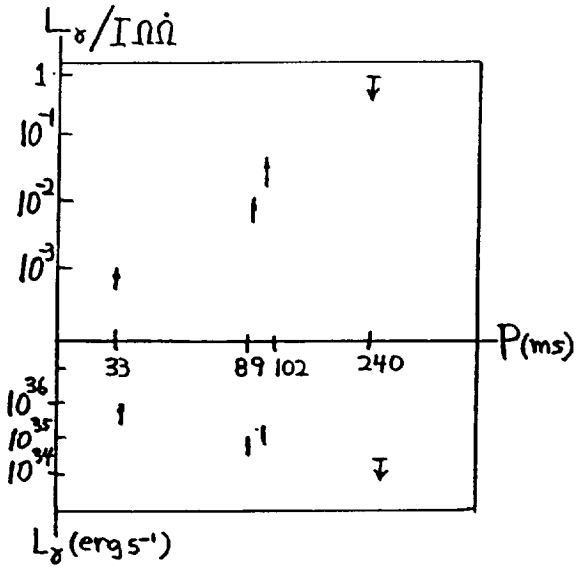

Fig. 2. The γ-ray luminosity (L_γ) and the ratio of L_γ to total spin-down power ($I\Omega\dot{\Omega}$) for the Crab, Vela, and Geminga pulsars and PSR 1706 – 44.

the direction to the observers. (The magnitude of $\vec{\mu}$ does not seem to vary much among the γ-ray pulsars). For the Crab pulsar, and then presumably for all, the γ-ray emission/accelerator region should be in the star's *outer*-magnetosphere. The Crab pulsar has strong optical pulses whose double subpulse structure coincides in shape and arrival time with those of its γ-rays. Therefore this emission is expected to come from the same local source as that for the γ-rays. The Crab's linearly polarized optical/IR luminosity is over 10^{-2} that of its γ-rays and over 10^{-5} that of its total spin-down power. Such an efficiency for optical radiation is not achieved within the magnetosphere by curvature acceleration, linear acceleration, or inverse Compton scattering on the pulsar radio beam[3]. This (as well as the polarization pattern[4] and the ratio of the optical to the X-ray intensity which has the same light curve) indicates that synchrotron radiation is the main optical source. The magnetic field which supports efficient sharply beamed synchrotron optical-IR emission must satisfy $eB\hbar/mc \ll 1$ eV. This inequality can be satisfied only at distances (r) from the Crab neutron star which satisfy the inequality $r \gg 3 \cdot 10^7$ cm $= 0.2 r_{\ell c}$ where $r_{\ell c} \equiv c\Omega^{-1}$ is the "light cylinder radius" where an exactly corotating magnetosphere would move at the speed of light.

A supporting argument, which also places the accelerator/emission region far from the star in the region near its light cylinder, follows from

the Crab pulsar's total X-ray/γ-ray power. The maximum net current which can flow between the star and its light cylinder is $J \sim \mu\Omega^2 c^{-1}$ and the upper bound for the power into γ-ray emission is $J\Delta V$ where ΔV is the potential drop (along $\vec{B}$) through the accelerator. For the Crab pulsar (with an assumed fan beam emission geometry) $\Delta V > 10^{14} V$. Such a large ΔV along $\vec{B}$ could not be maintained near the star; it would be quenched by an avalanche of $e^{\pm}$ pairs from γ-rays (curvature radiated by those same pairs) converting in the large polar cap magnetic field.

2. OUTER-MAGNETOSPHERE ACCELERATORS

The outer-magnetosphere near the light cylinder is still a region for which there is not yet a consensus on a detailed description. There are idealizations which unrealistically assume alignment of μ and $\vec{\Omega}$, no current flow, and no $e^{\pm}$ production regardless of the magnitude of the local electric field ($\vec{E}$) along $\vec{B}$[4,5]. These give a corotating magnetosphere near the star with a charge density[6]

$$\rho \simeq \vec{\Omega} \cdot \vec{B}/2\pi c, \tag{1}$$

and a competely empty region ("gap") much further out. In the former $\vec{E} \cdot \vec{B} = 0$ and (except for centripital acceleration) there is no acceleration of the charge separated magnetosphere plasma there. In the gap $\vec{E} \cdot \vec{B} \neq 0$ but there is no plasma to be accelerated. The gapless charge distribution around a non-aligned rotator when current flow is not permitted is shown in Fig. 3. When there are no magnetospheric sources of charge, but charge is allowed to flow from the magnetosphere, a different corotating stationary charge distirbution is achieved. The expected new charge distribution is sketched in Fig. 4. When all of the unrealistic constraints are abandoned e^- or e^+ may be expected to fill most of the outer-magnetosphere gap region in those pulsars which can self sustain $e^{\pm}$ pair production there. Such pair production would involve a bootstrapped symbiosis between γ-ray or X-ray poduction by synchrotron, inverse Compton, and curvature radiation by e^-/e^+ from $e^{\pm}$ production by intersecting γ-ray and γ-ray, X-ray or IR beams.[7,8,9] Unquenched particle acceleration regions, where $\vec{E} \cdot \vec{B} \neq 0$ despite the copious $e^{\pm}$ production in the outer magnetosphere, can exist only in places which are not effectively reached by crossing beams of radiation. The resulting "outer-gap" accelerator geometry is sketched in Fig. 5.

The inner boundary of the accelerator lies near the intersecion of the "null-surface" where $\rho = 0$ and the boundary of the "closed" field lines of the star on which magnetosphere current does not flow. The thickness of an outer-gap accelerator will grow until the $e^{\pm}$ production it sustains

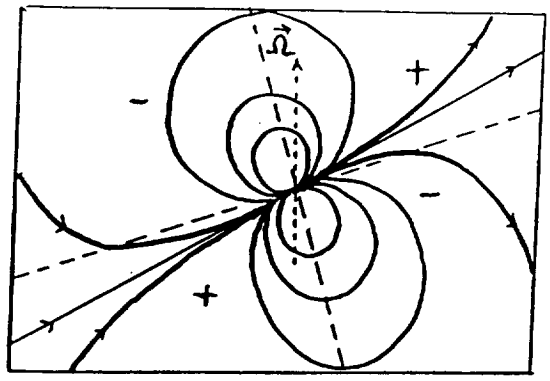

Fig. 3. Charge distribution around a rotating unaligned neutron star. The magnetosphere charge density vanishes on the "null-surface" indicated by the dashed lines on which $\vec{\Omega} \cdot \vec{B} = 0$.

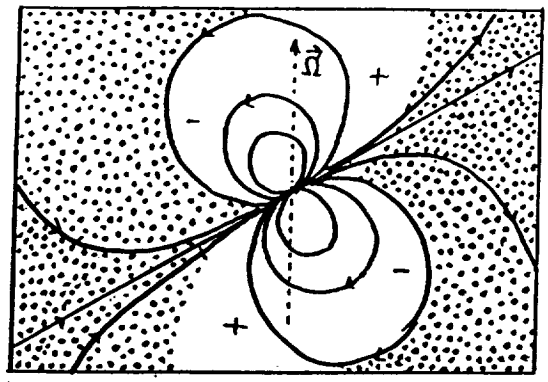

Fig. 4. The expected charge density around an inclined rotating neutron star with no magnetosphere currents. The dotted regions are empty of plasma.

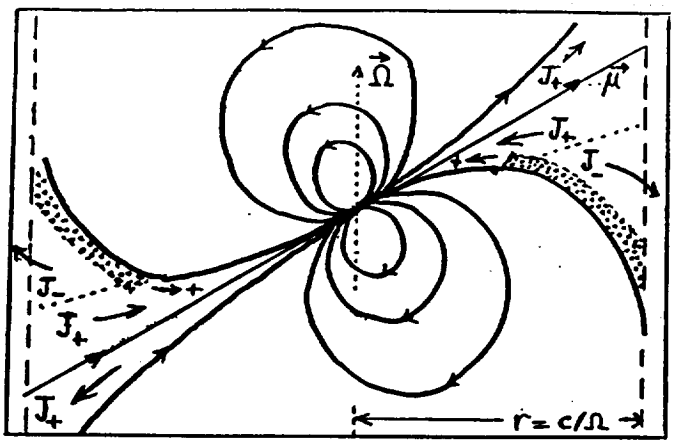

Fig. 5. Geometry and current flow of an outer-magnetosphere accelerator. One boundary of the gap is the last of the "closed" magnetic field lines which return to the stellar surface and do not reach the light cylinder. J is the current flow.

limits it while supplying the charged particles needed to complete the current flow in the magnetosphere through the null surface where $\vec{\Omega} \cdot \vec{B} = 0$.

Expected radiation beams from such an outer-gap accelerator are sketched in Fig. 6. Because of the $e^{\pm}$ production near the upper (lower) boundary of the RHS (LHS) outer-gap accelerator of Fig. 5, there is an apprroximate symmetry between radiation from the e^- and from the e^+ which flow oppositely within the accelerator and also from unseparated pairs which are formed outside of it. The accelerator and also radiation beams are emitted in both directions parallel to $\vec{B}$ from around the upper (lower) accelerator boundary. All beams with the same declination angle with respect to $\vec{\Omega}$ can be observable during a stellar rotation. Three potentially observable beams are indicated by 1, 2, and 3 in Figs. 6 and 7:

a) Beam 2 comes from curvature radiation by e^+ (or e^- if $\vec{\Omega} \cdot \vec{\mu}$ has the opposite sign) coming *toward* the stellar polar cap out of the near end of the RHS accelerator. It should have a spectral break near γ-ray energies of $\sim 10^2$MeV or larger.

b) Beam 1 consists of some curvature radiation directly from *outflowing* e^- in the accelerator (or from e^- flowing out from its far end) together with synchrotron radiation (and some inverse Compton scattering) from pairs produced above the accelerator. The synchrotron radiation will have a much lower energy spectral break (because of the interval between pair production and emission of such radiation) than that of beam 2 curvature radiation.

c) Beam 3 is an approximate mirror image of beam 1 from the e^+ and $e^{\pm}$ pairs of the LHS accelerator which move along $\vec{B}$ *toward* the star.

Calculated[8] and observed[9] spectra suggest associating beams 1 and 3 of Fig. 6 with those of Fig. 1 and beam 2 of Fig. 6 with the "interpulse" 2 of Fig. 1.[10] Because of plasma inertia and gap induced $\vec{E} \cdot \vec{B}$, the velocity directions of γ-ray emitting e^- and e^+ are not known on the open field lines where r approaches the light cylinder radius. Consequently, accurate arrival phases for beams 1, 2, and 3 are not, at present, predictable. An oversimplified model[6] suggests that the large $\Delta\phi \sim 0.4$ of the Crab and Vela pulsars (and also their cusp-like sub-pulse shapes) comes from an emission radius $r \sim 2r_{lc}/3$. [Romani, Chiang, and Ho[11] assume a $\vec{B}$ near the light cylinder exactly equal to that from a rotating dipole with no magnetosphere at all. Then a single field line from the star to the light cylinder may pass through the same inclination angle (with respect to $\vec{\Omega}$) several times before leaving the magnetosphere (e.g. at the points 1′ in Figs. 6 and 7). In their model the sources for emission

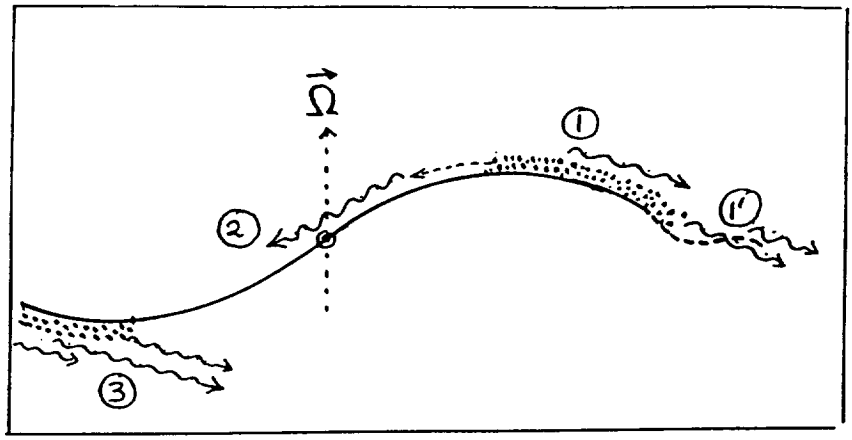

Fig. 6. Possible radiation beams from an outer-gap accelerator. All beams shown can have the same dip angle with respect to $\vec{\Omega}$.

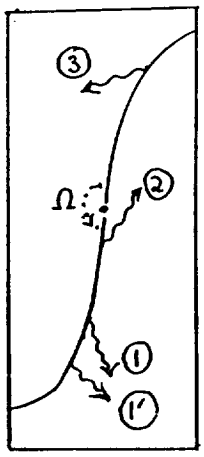

Fig. 7. A view of the emission beams of Fig. 6 from the spin axis direction which suggests the different aberration angles and effects of $\vec{B}$-line bending.

into beams 1, 2, and 3 of Fig. 1 are assumed to be from particle *outflow* from these special places on the same field line.]

3. DEATH VALLEY

As Ω decreases in a spinning-down pulsar the light cylinder radius expands and a self-sustaining outer-gap accelerator grows both in absolute thickness and in the fraction of the open field line bundle it occupies. A larger fraction of the stellar spin-down power must be expanded to maintain the $e^{\pm}$ production needed to sustain magnetospheric current flow between the star's polar cap and light cylinder. Almost all of this expended power is radiated away as γ-rays. Estimates[12,13] for the ratio $L_\gamma/I\Omega\dot{\Omega}$ of pulsars with aligned $\vec{\mu}$ and $\vec{\Omega}$ are shown in Fig. 8. As the

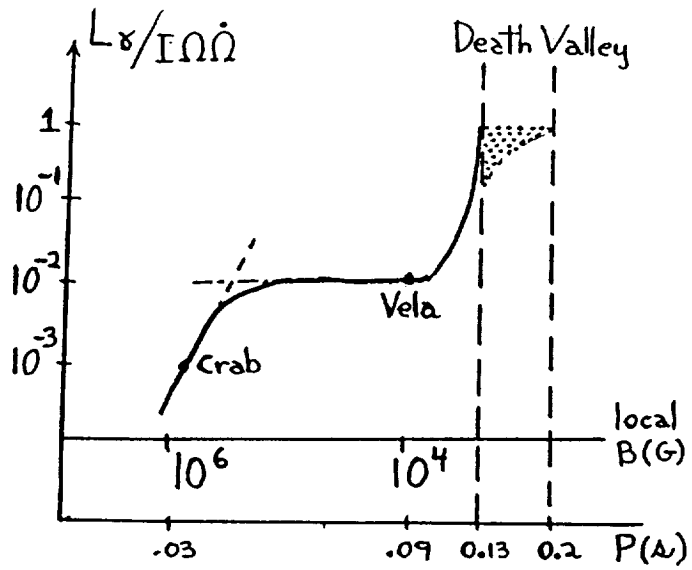

Fig. 8. A model calculation of the evolution of the ratio $L_\gamma/I\Omega\dot{\Omega}$ for a nearly aligned pulsar as it spins-down[12,13]. The two death lines correspond to inserting the accelerator's magnetic field B at $r = c/\Omega$ ($P = 0.13$ s) for which the Crab evolution is plotted and at $r = c/2\Omega$ ($P = 0.2$ s). The dotted region of the plot within Death Valley contains those values of P and L_γ which would give $L_\gamma \sim 4 \cdot 10^{35} - 5 \cdot 10^{36}$erg s^{-1}, the γ-ray luminosities indicated for the remaining unidentified Cos B sources[17].

spin down period P slows to about 10^{-1} s L_γ approaches $I\Omega\dot{\Omega}$. The absolute value of L_γ is then around that estimated for most of the still unidentified Cos B sources[14]. At still longer periods L_γ is expected to be largely quenched as the accelerator can no longer sustain itself. Just where the strong γ-ray emission should expire depends sensitively on the local B at the accelerator. Different death lines are found if B is evaluated as that at $r = r_{\ell c}$ or that at $r = r_{\ell c}/2$. Both are shown. When the angle between $\vec{\mu}$ and $\vec{\Omega}$ is large both underestimate the period at which an outer-gap accelerator is no longer a powerful γ-ray source.

4. GEMINGA

Several questions are raised by the identification of Geminga as a γ-ray pulsar.

a) Why is it such a strong γ-ray source, probably with an L_γ comparable to that of Vela, when its longer period and smaller $|\vec{\mu}|$ put it somewhat past the Death Valley of Fig. 8[13]?
b) Why is its subpulse separation $\Delta\phi$ so close to 0.5?

c) Why is it not seen as a radiopulsar?

Simple answers to all of these would follow from assuming that Geminga is, in most respects, a Vela-like pulsar except that its $\vec{\mu}$ is much more inclined to its $\vec{\Omega}$.

An outer-gap accelerator begins where the null surface ($\vec{\Omega} \cdot \vec{B} = 0$) intersects the boundary between a star's open and closed field lines. For an aligned $\vec{\mu}$, $r_{\rm ns}$, the minimum r where this occurs is $2r_{\ell c}/3$. When the angle between $\vec{\mu}$ and $\vec{\Omega}$ is large

$$r_{\rm ns} \sim \frac{4|\vec{\mu} \cdot \vec{\Omega}|^2}{9|\vec{\mu} \times \vec{\Omega}|^2} r_{\ell s} \qquad (2)$$

The magnitude of the local $\vec{B}$ around the beginning of an outer-magnetosphere accelerator gap can be about the same for Geminga and Vela if $\vec{\mu}$ is differently inclined with respect to $\vec{\Omega}$ in each. If the inclination angles is, say, 30° in Vela and about 65° in Geminga, B at $r = r_{\rm ns}$ is about the same for both. To sustain the needed outer-magnetosphere pair production and accelerator current (J_a) in Vela requires an accelerator there which spans about 10^{-1} of the open field line bundle between the star and the polar cap[8]. The electric field along $\vec{B}$ in the accelerator ($\vec{E}_a \cdot \hat{B}$) is also about 10^{-1} of that which would exist if the accelerator gap spanned the entire available open field line bundle. One consequence is that for the radiated power from Vela's outer-gap $L_\gamma \sim 10^{-1} \times 10^{-1} I\Omega\dot{\Omega}$. But if Vela sustains its needed outer-magnetosphere accelerator in the local B with those values of accelerator J_a and $\vec{E}_a \cdot \hat{B}$, the more inclined Geminga could do the same, as long as the fraction of available open field line flux needed to achieve them is less than one. Equivalently, Geminga can sustain a Vela-like outer-magnetosphere accelerator of the same power as Vela's if Geminga and Vela have similar $\mu r_{\rm ns}^{-3}$ and L_γ. For Geminga this would need $L_\gamma \sim I\Omega\dot{\Omega} \sim 5 \cdot 10^{34}$erg s^{-1}.

The smaller $r/r_{\ell c}$ and Ω of Geminga would result in some significant differences in geometry and spectra relative to Vela's outer-gap emission.

a) Because Geminga's gap fills it accessible open filed line bundle while Vela's fills only 10^{-1} of its, the relevant strengths of beams 1, 2, and 3 in Fig. 4 will change. The intensity of beam 2 would be expected to increase relative to that of the synchrotron part of beams 1 and 3. (Synchrotron radiation comes mainly from the boundary region *outside* the accelerator, and may no longer be the dominant contribution to L_γ.)

b) Because the radial distance to Geminga's emission region (r_e) is so much smaller relative to its $r_{\ell c}$ than is the case in Vela, the aberration and time of flight effects which determine the phase separation

of beams 1 and 3 are greatly diminished. For Geminga beams 1 and 3 will merge with a separation

$$\delta \sim 2r_e/\pi r_{\ell c} \tag{3}$$

and for beams 1 and 2

$$\Delta\phi = 0.5 + \delta. \tag{4}$$

Geminga's observed $\Delta\phi$ and pulse widths suggest $r_e \lesssim 5 \cdot 10^{-2} r_{\ell c} \sim 5 \cdot 10^7$ cm which would need Geminga's inclination angle to be at least 65°.

c) If curvature radiation does become the dominant contributor to the observed beams, the low energy spectral breaks in Geminga's spectrum should be at or above 10^2 MeV, much higher than those in Vela's two (mainly synchrotron) subpulses. Geminga's spectrum should resemble that of Vela's "interpulse" (region 2 in Fig. 1). This may already have been observed by Cos B[10].

5. SURFACE X-RAY RADIATION

Beams of very energetic e^+ (or e^-) will flow toward the Geminga or Vela neutron star polar caps from the starward ends of their outer-magnetosphere accelerators. While moving to the star such leptons will lose most of their energy to curvature γ-rays (beam 2 of Fig. 6) but will still hit each of the two polar caps with a power $L_{\rm pc} \sim 2 \cdot 10^{32}$erg s^{-1}. The impacted part of each polar cap would then have a temperature $kT_{\rm pc} \sim 0.5$ keV. The total soft X-ray luminosity from Vela[16] is, indeed, about $5 \cdot 10^{32}$erg s^{-1} and that from Geminga[15] seems likely to be quite comparable. However, the effective area for most of this emission is nearly the whole surface area of the star instead of that of the very much smaller (by a factor $\sim 10^{-4}$) polar caps. For Geminga almost all of the soft X-ray emission is at $kT \sim 0.04$ keV. Only a small fraction, about $4 \cdot 10^{-2}$, is emitted with $kT \sim 0.3$ keV (Fig. 9)[15].

Just such a transfer of power from a hot polar cap to the cooler rest of the neutron star surface is expected when $\vec{\mu}$ is strongly inclined with respect to $\vec{\Omega}$. When this is the case, parts of beams 2 and 3 of Fig. 6 can pass within 10^7 cm of the neutron star. There, beam γ-rays of energy $\gtrsim 3 \cdot 10^2$ MeV will be converted into $e^\pm$ pairs by the stellar magnetic field. These pairs will, in turn, synchrotron radiate lower energy γ-rays (typically with energy $\gtrsim 3$ MeV) very many of whch will convert to produce a larger, second generation of pairs much closer to the star. The circumstellar pair density would not be sufficient to

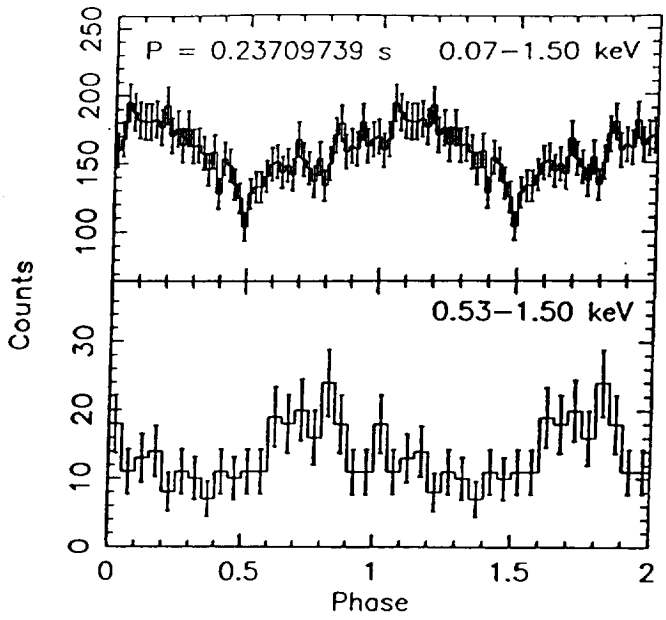

Fig. 9. Soft X-ray light curves of Geminga[15].

affect keV polar cap X-rays were it not for the strong magnetic field near the star. At $r \sim 3R$ where $B \sim 10^{11}$G the cross section for X-ray scattering at $\hbar\omega = 1$ keV is resonant with $\int \sigma d\omega = (2\pi)^2 e^2/mc$. This leads to estimates supporting the following account of the escape of keV polar cap X-rays from Geminga (and perhaps Vela).

1) Almost all keV polar cap X-rays are backscattered by resonant scattering on abundant $e^{\pm}$ pairs at $r \sim 3R$.

2) These X-rays, usually after multiple reflections, hit the stellar surface which reemits them at $kT \sim 10^{-1} kT_{\rm pc} \sim 10^{-1}$keV. The much softer X-rays from the whole surface pass easily through the reflecting screen at $r \sim 3R$ and, perhaps after some reflection, through their own resonant $e^{\pm}$ scattering layer at $r \sim 6R$.

3) That small fraction of keV polar cap X-rays whose polarizaiton is almost exactly parallel to the $\vec{B}$ they traverse at $r \sim 3R$ will have only the non-resonant Thomson cross section for scattering on e^-/e^+. These will, therefore, escape without degradation in energy. This may be the observed weak hotter ($kT \sim 0.3$ KeV) pulsed component from Geminga whose luminosity is less than 10^{-1} that of the softer ($kT \sim 4 \cdot 10^{-2}$ KeV) component. (Its single component light curve is consistent with a sunspot-like geometry for the polar caps. Such a geometry has also been suggested for other reasons[17].)

A pair-filled magnetosphere, which seems a necessary consequence

of a powerful outer-gap acceleator in a sufficiently inclined γ-ray pulsar, may be the origin of other features in the observed emission from Geminga.

a) The densest near-magnetosphere pair density would be expected around (and within) the open field line bundle. The soft 0.1 KeV X-ray $e^{\pm}$ resonant cross section at $r \sim 6R$ should then result in a partial stellar eclipse during each rotation (Fig. 10) which reduces the observed X-ray luminosity by a fraction $\sim (\Omega R/c)(r/R)^3 \sim 0.2$. This may be the origin of the light curve minimum in Fig. 9 at phase $\phi = 0.5$. If so, that dip should be found to coincide in phase with one of Geminga's two γ-ray subpulses.

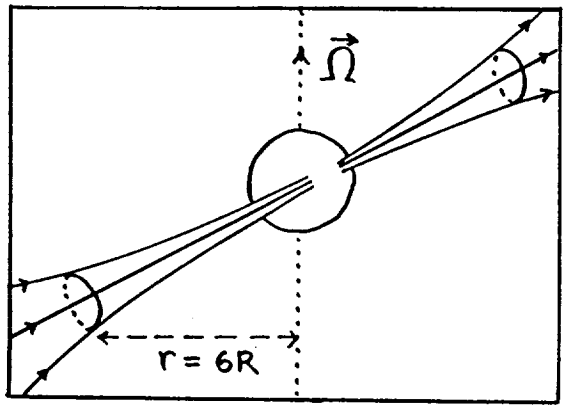

Fig. 10. Soft X-ray eclipse geometry of the Geminga neutron star by the open field line resonant reflection disk at $r \sim 6R \sim 6 \cdot 10^6$cm.

b) If the near-magnetosphere $e^{\pm}$ density within the entire open field line bundle exceeds the Goldreich-Julian density there, then any polar cap accelerator which might otherwise form in that bundle would be quenched. The radio emission which is generally thought to be associated with such acclerators would then be absent. (This might also explain the relative absence of observed radiopulsars with $B \sim$ several $\cdot 10^{12}$G and periods slightly less than Geminga's.)

ACKNOWLEDGEMENTS

This is contribution number 510 of the Columbia Astrophysics Laboratory. MR wishes to acknowledge support for this work under NASA Grant NAG5-2016 and NSF Grant AST89-01681.

REFERENCES

1. J. Halpern, in preparation (1992).
2. C. Fichtel *et al.*, these proceedings.
3. M. Ruderman in *Particle Acceleration Near Accreting Compact Objects*, J. van Paradijs, M van der Klis and A. Achtenberg, eds. (North Hollandm Amsterdam) (1991).
4. J. Krause-Polstorff and F.C. Michel, *M.N.R.A.S.*, **213**, 43 (1985).
5. K.S. Cheng and M. Ruderman, *Ap.J.*, **373**, 187 (1991).
6. P. Goldreich and W. Julian, *Ap.J.*, **157**, 869 (1969).
7. K.S. Cheng, Cheng Ho, and M. Ruderman, *Ap.J.*, **300**, 500 (1986).
8. K.S. Cheng, Cheng Ho, and M. Ruderman, *Ap.J.*, **300**, 502 (1986).
9. Cheng Ho, Los Alamos Workshop on Isolated Pulsars, Taos, NM, in press (1992).
10. I. Grenier, W. Hermsen, and C. Hote, *Adv. Space. Res.*, **11 (8)**, 107 (1991).
11. R. Romani, J. Chiang, Cheng Ho, these proceedings.
12. M. Ruderman and K.S. Cheng, *Ap.J.*, **335**, 306 (1988).
13. K. Chen and M. Ruderman, *Ap.J.*, in press (1992).
14. H.A. Mayer-Hasselwander and G. Simpson, *Adv. Space Res.*, **10(2)**, 89, (1990).
15. J. Halpern and S. Holt, *Nature*, **357**, 222 (1992).
16. H. Ögelman, J.P. Finley, and H.U. Zimmerman, preprint (1992).
17. K. Chen, K.S. Cheng, and M. Ruderman, in preparation.

THE ASTROPHYSICAL JOURNAL, 415:286–297, 1993 September 20

SOFT X-RAY PROPERTIES OF THE GEMINGA PULSAR

J. P. HALPERN AND M. RUDERMAN
Columbia Astrophysics Laboratory, Columbia University, 538 West 120th Street, New York, NY 10027
Received 1992 December 28; accepted 1993 March 26

ABSTRACT

The *ROSAT* soft X-ray spectrum and pulse profile of the Geminga pulsar are analyzed and interpreted in terms of thermal emission from the surface of the neutron star. The X-ray spectrum appears to consist of two blackbody components with $T_1 = (5.2 \pm 1.0) \times 10^5$ K and $T_2 \sim 3 \times 10^6$ K, respectively. The inferred ratio of surface areas, A_2/A_1, is $\sim 3 \times 10^{-5}$. Both components are highly modulated at the pulsar rotation period, but the harder X-ray pulse is narrower, and leads the main (soft) X-ray pulse by $\sim 105°$ of phase. The soft X-ray component is interpreted as photospheric cooling of much of the neutron star's surface area, while the small, hot region could be part of the much smaller polar cap heated by energetic particles flowing inward from the magnetospheric accelerator which is responsible for the production of Geminga's γ-rays. Geminga's γ-ray emission is consistent with outer-magnetosphere accelerator models for highly inclined dipoles. These predict the beaming of energetic γ-rays close enough to the star to give copious $e^{\pm}$ production in the stellar magnetic field and a large circumstellar pair density from pair inflow toward the surface. These pairs may quench radio emission and also reflect most of the hard polar cap X-rays back to the stellar surface by cyclotron resonance scattering. They are then reemitted from that much larger area at the lower temperature T_1. The single-peaked nature of the X-ray pulse and its energy-dependent phase suggest an off-center dipole geometry for the *surface* magnetic field.

Under the assumption that the soft X-ray emission comes from the full surface of a neutron star of radius $R = 10$ km, a distance estimate of (150–400) pc is derived. This range is consistent with the fitted interstellar column density of $(1.5 \pm 0.5) \times 10^{20}$ cm^{-2}. Distances less than 150 pc are probably ruled out both by the lower limit on the column density, and also by the requirement that the Rayleigh-Jeans extrapolation of the soft X-ray spectrum not exceed the observed blue flux of the faint optical counterpart. This distance estimate implies that Geminga's efficiency for converting spin-down power into γ-rays is near unity, and that there may be significant beaming of the the γ-rays as well. These results tend to bolster the prospect that most of the unidentified high-energy γ-ray sources in the Galactic plane are pulsars, some of which may be radio quiet.

Subject headings: gamma rays: observations — pulsars: individual (Geminga) — stars: neutron — X-rays: stars

1. INTRODUCTION

The high-energy γ-ray source Geminga (2CG 195+04, 1E 0630+178) is a radio-quiet pulsar with period $P = 0.237$ s, surface field $B_p \sim 1.6 \times 10^{12}$ G, and characteristic age $\tau = P/2\dot{P} = 3.4 \times 10^5$ yr (Halpern & Holt 1992; Bertsch et al. 1992). Its soft X-ray properties contain a great deal of information about thermal emission from the surface of the neutron star. There are very few pulsars for which the bulk of the soft X-ray emission is demonstrably photospheric, and it is argued here that Geminga is one of the more secure cases. Therefore, it can be used to test theories of neutron star cooling, polar-cap heating, and the effect of the surface magnetic field and environment on the emergent spectrum. Other pulsars for which such surface emission is likely to contribute substantially are PSR 0656+14 (Córdova et al. 1989; Finley, Ögelman, & Kizloğlu 1992), PSR 1055−52 (Cheng & Helfand 1983; Brinkmann & Ögelman 1987), and Vela (Ögelman, Finley, & Zimmermann 1993), but Geminga allows the most detailed examination so far of the spectrum and pulse properties of the photospheric emission.

If interpreted as blackbody emission, the X-ray spectrum also provides the only measurement of the distance to Geminga, which is crucial to the determination of the efficiency for turning spin-down power into γ-rays. This is turn affects the likelihood that the other unidentified Galactic high-energy γ-ray sources are pulsars. Geminga bolsters the hypothesis that the *COS B* sources are a population of efficient γ-ray pulsars. The X-ray pulse profile of Geminga is complex and highly modulated, and to the extent that it can be interpreted in terms of the geometry of the magnetic field, it may help in understanding the γ-ray emission mechanism and pulse profile. This paper presents a more comprehensive analysis of the *ROSAT* observation of the Geminga pulsar than was possible in the initial report by Halpern & Holt (1992). Although the data are the same, a number of additional results have been obtained, and the interpretation also incorporates properties of the γ-ray emission.

2. PULSE PROFILE AND TIMING

A more detailed soft X-ray pulse profile was constructed by folding about the revised *EGRET* ephemeris (P and $\dot{P}$) of Mayer-Hasselwander et al. (1992), which is more precise than the original X-ray determination. Table 1 gives the folding parameters which apply to the epoch of the *ROSAT* observation in the Barycentric Dynamical Time (TDB) system. A total of 7911 counts in the 0.07–1.50 keV band, of which less than 2% are background, were extracted from a circle of radius 150″ in the position sensitive proportional counter. Figure 1 shows a number of details that were not apparent in the original examination of the X-ray data. First, there is apparently a sharp dip in the soft X-ray flux, and possibly significant high-frequency structure, especially on the rising side of the pulse. A

TABLE 1

GEMINGA PULSE EPHEMERIS

Parameter	Value
T_0 (JD)[a]	2,448,329.886823149
P (s)	0.2370973861
$\dot{P}$ (s s^{-1})	1.0977×10^{-14}

[a] TDB time of phase 0 in Figs. 1 and 2.

revised estimate of the pulsed fraction in the 0.07–0.28 keV band is 33%. Although it appeared in Halpern & Holt (1992) that the pulsed fraction decreases with energy, it is now seen that there is actually a faint but highly modulated pulse at energies around 1 keV which leads the peak of the main X-ray pulse by $\sim 105°$ of phase. The weakness of the modulation around 0.5 keV is due to the fortuitous superposition of these two out-of-phase components, and it appears that both components are individually highly pulsed in a roughly energy-independent manner. We shall refer to the ~ 0.2 keV X-rays and the ~ 1 keV X-rays as the "soft" and "hard" components, respectively. The pulsed fraction of the hard X-rays is $\sim 37\%$, similar to that of the soft X-ray pulse, but the hard pulse is narrower. The dip at phase 0.5 is not apparent in the hard light curve, although the photon statistics here are quite poor. The spectral analysis presented in the next section lends additional

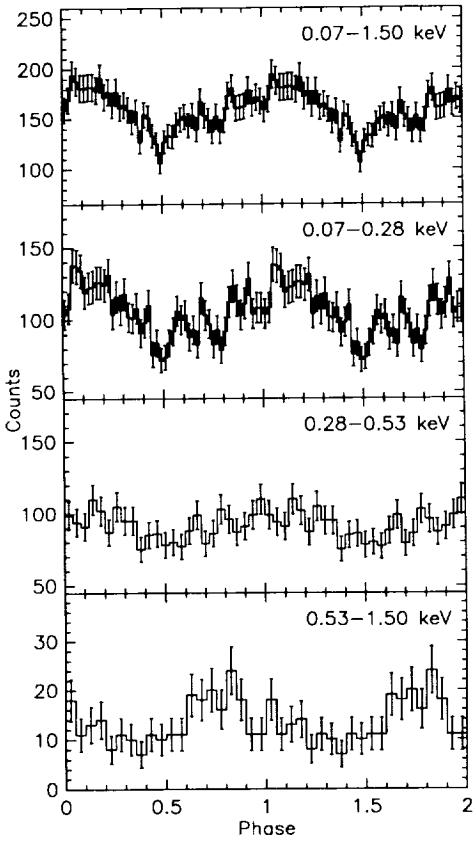

FIG. 1.—X-ray pulse profile folded according to the ephemeris of Table 1. The top panel shows all the data in the 0.07–1.5 keV range, and the lower three panels show the same data separated into three energy bands. The data are repeated for two cycles to guide the eye. Phase 0.0 corresponds to T_0 from Table 1.

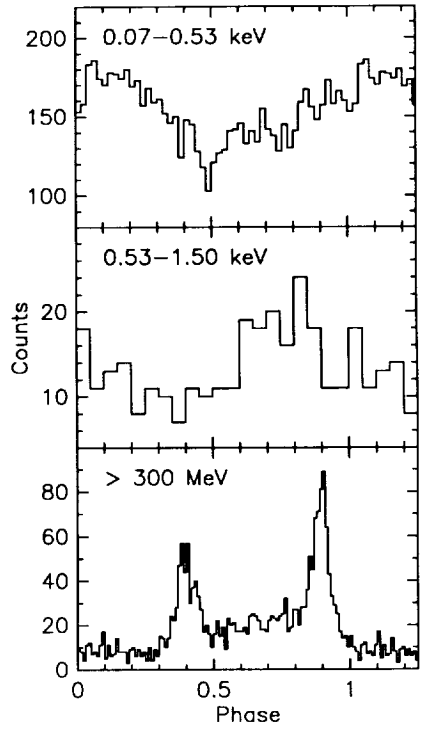

FIG. 2.—A comparison of the X-ray and γ-ray pulses in absolute phase. Phase 0.0 corresponds to T_0 from Table 1. The γ-ray light curve is taken from Bertsch et al. (1992).

support to the interpretation of the pulse profiles as two separate components. In particular, the soft component will be interpreted as emission from the full surface of the neutron star, while the hard X-ray pulse could arise from the heated polar caps.

The relative phasing of the X-ray and γ-ray pulses is of great interest, since the pulse profiles are so different. The best current analysis of the *ROSAT* spacecraft clock leads to the alignment shown in Figure 2. The time of phase 0.0 is given by T_0 in Table 1, which is an extrapolation of the *EGRET* ephemeris over the 5 week interval between the *ROSAT* observation and the first *EGRET* observation. The phase comparison using P and $\dot{P}$ should be accurate to better than 0.01 cycles in the absence of significant timing noise and is comparable to the accuracy of the *ROSAT* spacecraft clock (Ögelman et al. 1993). (It should be noted, however, that $\ddot{P}$ as given by Hermsen et al. [1992] and Mattox et al. [1992] probably *is* dominated by timing noise or cycle count errors, since the quoted values lead to unreasonably large values of the braking index, 31 and 44, respectively.) Another possible source of uncertainty is the positon of Geminga, which could cause an error of ≤ 7 ms (0.03 cycles) in the arrival time at the barycenter if it is off by $\leq 3''$ in right ascension. An error of this magnitude would be expected if the G'' optical counterpart (Halpern & Tytler 1988) is incorrect, or if there is exceptionally high proper motion. The detection of a proper motion for this star of $\simeq 0''.17$ yr^{-1} by Bignami, Caraveo, & Mereghetti (1993) obviates both of these concerns. More worrisome is a possible ambiguity of 0.5 *s* in the interpretation of the times from the *ROSAT* spacecraft clock (Ögelman 1992, private communication), which would result in an error of 0.11 cycles in the phase of the pulse. For

now, we tentatively accept the relative phasing of the X-ray and γ-ray pulses shown in Figure 2 as correct to within ~ 0.13 cycles.

The sharp, double-peaked γ-ray pulse is in marked contrast to the broad, single-peaked X-ray pulse. In § 5.2, it is argued that Geminga's high γ-ray efficiency and the 180° separation of its γ-ray peaks call for a highly inclined dipole. If so, the single hard X-ray pulse cannot be understood in terms of polar-cap emission from a dipole close to the center of the star, since both polar caps should be visible with a near 180° separation of their X-ray emission. The soft X-ray component is presumed to come from nearly the full surface of the star, and it too is single-peaked. The simplest resolution of this problem invokes an off-center dipole, as described in § 5.5, so that the polar caps are too close together to be resolved in the light curve of the rotating star. The γ-ray pulses originating in the outer magnetosphere can nevertheless be double fan beams which are visible from most directions. The hard X-ray pulse roughly coincides with the bridge of γ-ray emission between the two main peaks, which is consistent with an off-center dipolar configuration if the γ-rays are comining from regions along the open field lines which are roughly symmetric with respect to the polar caps.

3. SPECTRAL ANALYSIS

The X-ray source counts were extracted from a circle of radius 150″, and background from an annulus between radii of 150″ and 250″. A total of 7637 net counts were detected in the 0.08–2.45 keV band in a live time of 14,205 s. As shown by Halpern & Holt (1992), the spectrum cannot be fitted by a single blackbody or power law, both of which leave a residual hard excess above 0.6 keV. Two-component models are adequate, and one which is particularly amenable to interpretation is a pair of blackbodies,

$$F(E) = CE^3\left(\frac{1}{e^{E/kT_1}-1} + \frac{f}{e^{E/kT_2}-1}\right)e^{-\sigma(E)N_{\rm H}} \quad \text{keV cm}^{-2}\ \text{s}^{-1}\ \text{keV}^{-1}\ . \quad (1)$$

The interstellar medium photoelectric cross sections of Morrison & McCammon (1983) are used for $\sigma(E)$. The four fitting parameters are the temperatures T_1 and T_2, interstellar column density $N_{\rm H}$, and fraction f which is closely related to the ratio of surface areas (A_2/A_1) of the two blackbody components. (For each trial spectrum, the normalization constant C is fixed by the total counts, and its error is largely systematic.) A full four-dimensional χ^2 grid search was performed, and the best fit is shown in Figure 3.

Before interpreting these results, it is necessary to point out that there are a number of sharp features in the residuals between 0.2 and 0.4 keV which have been seen in other sources, and which are thought to reflect an as yet unsolved problem in the pulse-height analysis or the detector response matrix. These features are not all likely to be real, and they contribute to an unacceptable total χ^2 of 61 for 42 degrees of freedom. In the hope that the overall continuum shape is not significantly affected by this problem, a simple renormalization of the χ^2 values by the factor 42/61 was made to permit sensible confidence contours to be derived.

A number of interesting results can be drawn from this fit. First, the relative contributions of the two blackbodies cross over at ~ 0.6 keV, which is very close to the energy of minimum modulation as seen in the light curve (Fig. 1). This coincidence lends additional credence to the idea that two components are present in the X-rays, since they can be separated both spectrally and temporally. The lower tem-

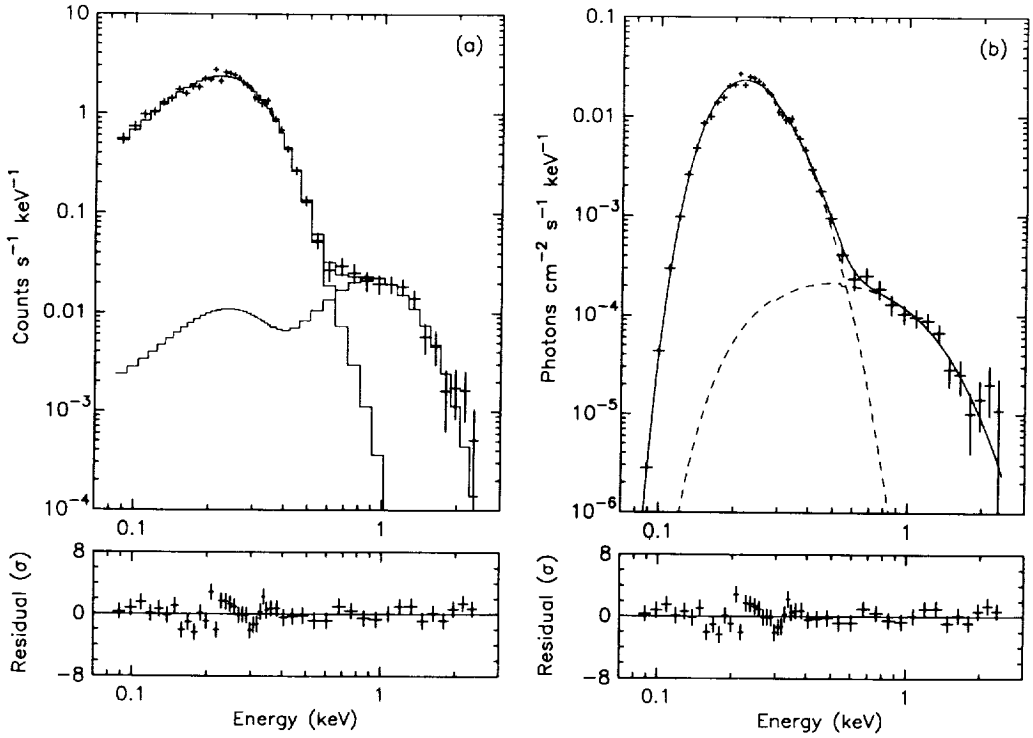

FIG. 3.—Fit of the double blackbody model to the X-ray spectrum of Geminga. (*a*) Raw counts and model spectra folded through the detector response matrix. (*b*) Unfolded spectral model.

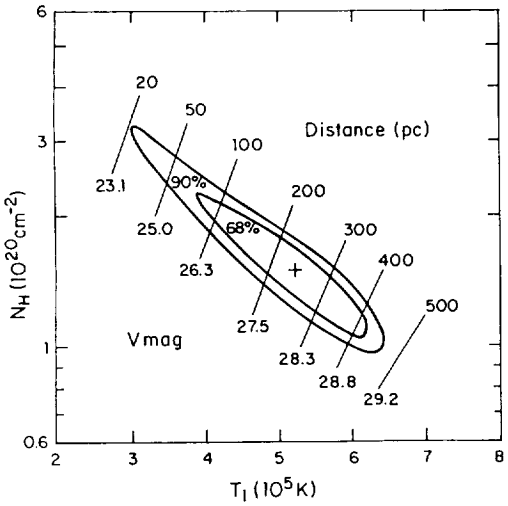

FIG. 4.—Confidence contours for the parameters of the soft X-ray component in the double blackbody fit. The confidence levels correspond to the case of three interesting parameters (T_1, N_H, and C). Visual magnitudes are extrapolated from the Rayleigh-Jeans tail of the blackbody fit, while distances assume emission from the full surface of a neutron star of radius $R = 10$ km.

perature blackbody with $T_1 \simeq 5 \times 10^5$ K accounts for $\sim 96\%$ of the bolometric flux, and its fit is relatively insensitive to the presence of the weaker hard component. If the χ^2 grid is projected onto the (T_1, N_H) plane, the confidence contours shown in Figure 4 restrict the temperature and column density to the ranges (3–6) $\times 10^5$ K and (1–3) $\times 10^{20}$ cm^{-2}, respectively. The confidence contours are elongated because the errors on T_1 and N_H are correlated. Further restrictions on these parameters are made possible by the incorporation of optical data as described in § 4 below.

A second interesting projection of the χ^2 grid is onto the (T_2, f) plane. Figure 5 shows that T_2 lies in the range (2.3–3.9) $\times 10^6$ K, and that the fractional area f is $\sim 3 \times 10^{-5}$. The very large range allowed for f, 10^{-6}–10^{-4}, is dominated not by the uncertainty in the flux of the hard component, but rather by the ranges in N_H, T_1, and normalization of the soft

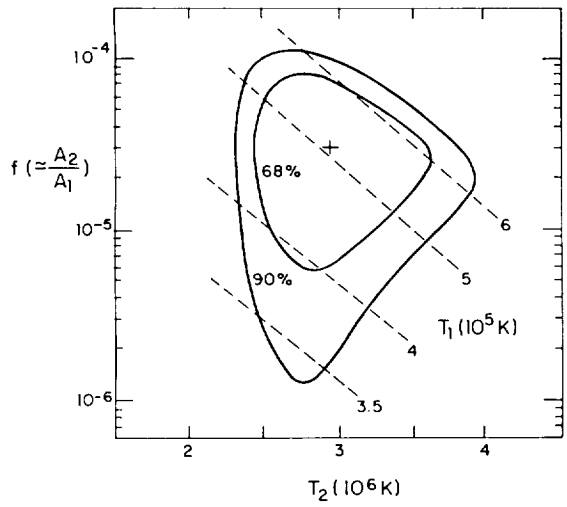

FIG. 5.—Confidence contours for the parameters of the hard X-ray component in the double blackbody fit. The confidence levels correspond to the case of two interesting parameters (T_2 and f). Corresponding values of T_1 are given as dashed lines.

TABLE 2

FIT TO DOUBLE BLACKBODY MODEL

Parameter	Value	Confidence (%)
T_1	$5.2\ (+1.0, -1.3) \times 10^5$ K	68
	$(+1.2, -2.2)$	90
T_2	$3.0\ (+0.7, -0.6) \times 10^6$ K	68
	$(+0.9, -0.7)$	90
N_H	$1.5\ (+0.8, -0.5) \times 10^{20}$ cm^{-2}	68
	$(+1.7, -0.6)$	90
f	$3.5\ (+4.5, -2.9) \times 10^{-5}$	68
	$(+6.6, -3.4)$	90
C	162	...
F_1[a]	7.2×10^{-12} ergs cm^{-2} s^{-1}	...
F_2[a]	2.6×10^{-13} ergs cm^{-2} s^{-1}	...

[a] Bolometric flux in component before interstellar absorption.

component since a large and uncertain fraction of the soft emission is absorbed in the intervening interstellar medium. Projections of the corresponding best fit values of T_1 are shown as dashed lines in Figure 5. A summary of the best fit spectral parameters is given in Table 2. The hard component is interpreted in § 5.3 in terms of polar-cap heating of an off-center dipole by an outer magnetosphere accelerator. A division of the pulse height spectrum into several time-resolved segments according to rotation phase demonstrates that each of the two components varies in an approximately energy-independent manner. That is, no variations in T_1 or T_2 are detectable as a function of rotation phase, although the paucity of counts above 0.5 keV precludes a meaningful test for variation in T_2.

A second not implausible two-component model of the X-ray spectrum consists of a blackbody plus a power law,

$$F(E) = C\left(\frac{E^3}{e^{E/kT_1} - 1} + f E^{-\alpha}\right) e^{-\sigma(E) N_H} \text{ keV cm}^{-2} \text{ s}^{-1} \text{ keV}^{-1}, \quad (2)$$

where α is the energy index. The best-fit spectrum is shown in Figure 6, and the parameters and uncertainties are listed in Table 3. The fit is nearly as good ($\chi^2 = 63$) as the double blackbody. Since the power-law component makes a small contribution to the total X-ray flux, the fit parameters for the soft blackbody are not significantly different from those in the double blackbody model. Although the best fit T_1 is changed slightly, the confidence contours encompass the same range of

TABLE 3

FIT TO BLACKBODY PLUS POWER-LAW MODEL

Parameter	Value	Confidence (%)
T_1	$4.5\ (+1.4, -1.5) \times 10^5$ K	68
	$(+1.6, -2.1)$	90
α	$1.47\ (+0.28, -0.37)$	68
	$(+038, -0.55)$	90
N_H	$1.85\ (+1.3, -0.7) \times 10^{20}$ cm^{-2}	68
	$(+2.4, -0.8)$	90
f	$1.93\ (+9.1, -1.9) \times 10^{-7}$	68
	$(+12.1, -1.9)$	90
C	545	...
F_1[a]	1.1×10^{-11} ergs cm^{-2} s^{-1}	...

[a] Bolometric flux in blackbody component, before interstellar absorption.

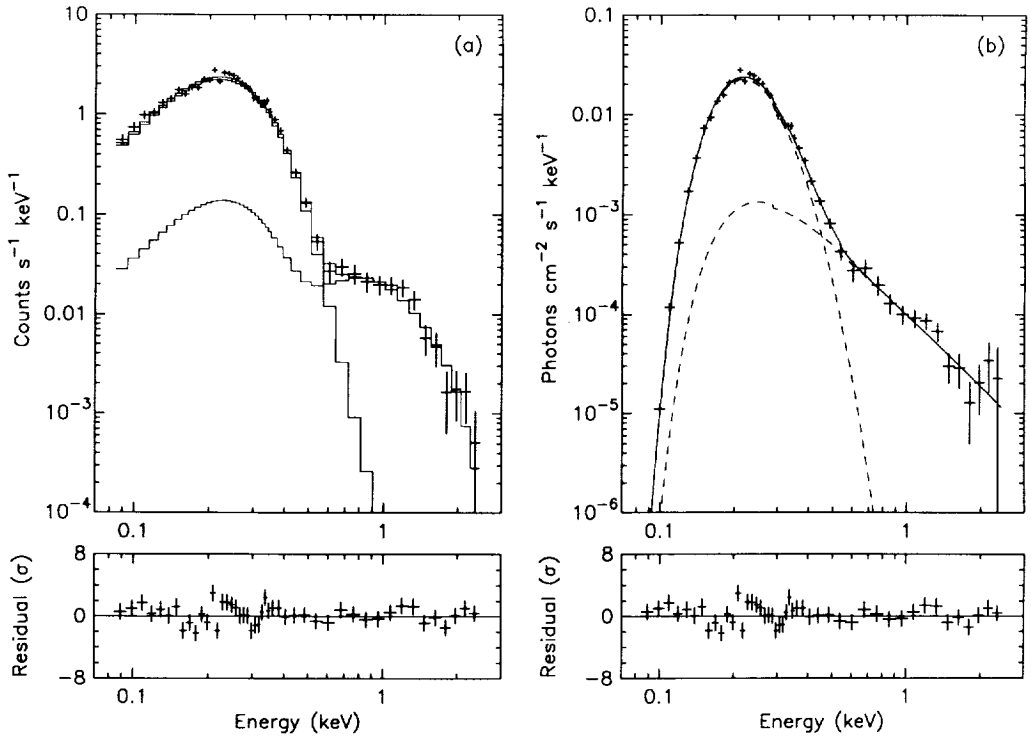

FIG. 6.—Fit of the blackbody plus power-law model to the X-ray spectrum of Geminga. (*a*) Raw counts and model spectra folded through the detector response matrix. (*b*) Unfolded spectral model.

parameters, as shown in Figure 7. An extrapolation of the power-law component with $F(E) \propto E^{-1.5}$ to the visible would exceed the flux of the 25 mag G″ optical counterpart (Halpern & Tytler 1988) by a factor of several hundred. If the hard component were to be interpreted as synchrotron emission from the magnetosphere, the local magnetic field must be such that the low-frequency cutoff at $\omega = eB/mc$ lies above the optical band. This implies that $B > 10^9$ G. Therefore, any X-ray synchrotron emission would have to arise from within 10 stellar radii of the surface of the neutron star. Synchrotron self-absorption is not an alternative explanation for the weakness of the optical emission, since $\nu_{abs} < 10^{13}$ Hz for this component. Although formally acceptable, a synchrotron origin for the hard X-rays seems less attractive than surface emission because it is difficult to understand why magnetospheric emission far from the stellar surface should have a single-peaked pulse. Regardless of the nature of the hard X-rays, the weak optical flux *could* be synchrotron emission coming from radii *larger* than 10^7 cm. The optical flux in the visible band is only 1.7×10^{-15} ergs cm^{-2} s^{-1}, which is a factor of 100 less than that of the "hard" X-ray component at 1 keV.

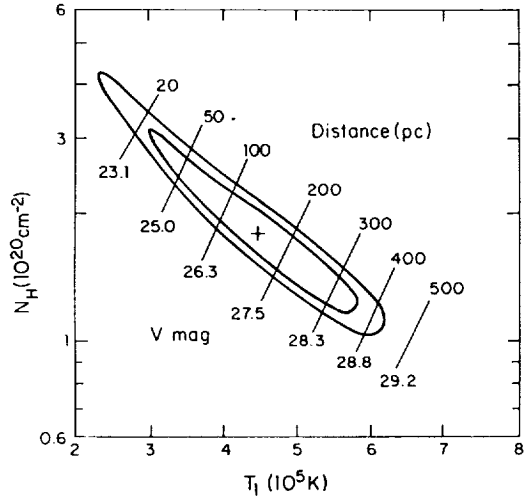

FIG. 7.—Confidence contours for the parameters of the soft X-ray component in the blackbody plus power-law fit. The confidence levels corresponds to the case of three interesting parameters (T_1, N_H, and C). Visual magnitudes are extrapolated from the Rayleigh-Jeans tail of the blackbody fit, while distances assume emission from the full surface of a neutron star of radius $R = 10$ km.

4. DISTANCE TO GEMINGA

The softer X-ray component currently provides the only measurement from which the distance to Geminga can be inferred. Several constraints on the distance are associated with the spectral fit. For each point in Figure 4, the normalization constant C can be converted to a visual magnitude by extrapolation of the Rayleigh-Jeans tail of the X-ray spectral fit. If we assume in addition that the X-ray emission comes from the full surface of a neutron star of radius $R = 10$ km, then a distance can be assigned to each fit. The straight lines of Figure 4 indicate these predicted optical magnitudes and distances. Although all the information in Figure 4 is derived purely from the X-ray spectrum, a number of additional constraints can be brought to bear to further restrict the allowed range of parameters. First, the G″ optical counterpart has magnitudes $V = 25.2 \pm 0.3$ (Halpern & Tytler 1988) and $B = 26.5 \pm 0.5$ (Bignami, Caraveo, & Paul 1988). Since the $B - V$ color is redder than Rayleigh-Jeans, it would be unreasonable for the extrapolated X-ray spectrum to exceed the optical brightness. This would seem to rule out distances smaller than 150 pc in Figure 4. (Although Bignami et al. [1993] noted that their measured proper motion is *consistent*

with a distance of 100 pc, the *uncertainty* which must be associated with the use of proper motion as a distance estimator is at least a factor of 3. The proper motion is therefore not inconsistent with our own lower limit on the distance of 150 pc.)

Additional restrictions on the distance can be gleaned from the measured interstellar column densities in the direction of Geminga. These come principally from absorption-line studies of nearby stars; the derived column densities as a function of distance in the Galactic plane have been summarized by Paresce (1984) and Frisch & York (1983). The column density toward Geminga is small, but it is poorly determined because very few stars have been studied, and this direction grazes the edge of the local bubble which is devoid of neutral material to large distances in the third Galactic quadrant. What can be most reliably extracted from these surveys (in particular, from Fig. 1 of Frisch & York and Fig. 4 of Paresce) is that N_H does not rise to 1×10^{20} cm^{-2} until a distance of at least 150 pc is reached. It is also possible that a distance of ~ 500 pc is necessary for N_H to reach this value. So the allowed range of distances can conservatively be restricted to 150–450 pc by comparing the X-ray spectral fit in Figure 4 with these published measurements of the local interstellar column density.

A final restriction on the distance comes from the requirement that the apparent γ-ray luminosity not exceed the spin-down power $I\Omega\dot{\Omega}$, or at least not greatly, since some beaming is possible. The implied upper limit is ~ 400 pc (Bertsch et al. 1992). So when all the constraints are combined, the best estimate of the distance to Geminga is 250 pc, with an allowed range of 150–400 pc. The corresponding range of X-ray spectral parameters in the restricted space of Figure 4 is $T_1 = (5.2 \pm 1.0) \times 10^5$ K, and $N_H = (1.5 \pm 0.5) \times 10^{20}$ cm^{-2}.

Of the assumptions that could affect this distance estimate, one might at first suspect the "full surface" condition, since if the assumed area of the emitting surface is incorrect, the distances indicated in Figure 4 are changed. But in fact, the acceptable *range* of distances is insensitive to changes in the effective emitting area. Although the individual distance contours indicated in Figure 4 would change, the extrapolated optical magnitudes cannot. Neither would the fitted N_H, the observed interstellar column densities, or the γ-ray efficiency limit. Similarly, the assumed form of the "hard" X-ray component does not significantly affect the fit to the soft component, so the distance limits indicated in Figure 7 are the same as those in Figure 4. The *combination* of conditions restricting the distance to between 150 and 400 pc is quite robust, and a much more accurate determination of the X-ray spectral parameters would have to be made before the uncertainty in distance could be reduced. A better determination of the actual run of column density versus distance in the direction toward Geminga would also be helpful in pinning down the distance. If the distance estimate presented here is flawed, it is more likely to be a result of gross errors in the detector response matrix, or substantial deviations of the spectrum from a blackbody as considered in § 5.4, neither of which are obviously present.

5. INTERPRETATIONS

5.1. *Into the Valley of Death*

Similarities among the γ-ray spectra and most of the light curves of the known γ-ray pulsars (Crab, Vela, PSR 1706−44, Geminga) suggest that a similar, powerful accelerator is operating in each of their magnetospheres. If this is indeed the case, such an accelerator would have to be located in their outer magnetospheres ($r \gg R \sim 10^6$ cm). This would almost certainly be true for the source of the Crab pulsar's optical radiation. Synchrotron emission seems to be the only (incoherent) mechanism which is powerful enough to produce the Crab's optical light, and the radiating $e^{\pm}$ pairs must move relativistically to give the sharply peaked light curve. This limits the local magnetic field to $B \lesssim 10^8$ G, which is found only near the light cylinder, at $r_{lc} = c/\Omega \sim 10^8$ cm. But the arrival phase of each of the Crab's two optical pulses is identical to those of its X-rays and γ-rays. This strongly implies a common geometrical location for all of the radiation very far from the stellar surface.

Independent arguments for an outer-magnetosphere accelerator comes from the *COS B* and *EGRET* observations of Geminga. First, γ-ray emission remains strong up to 5 GeV (Grenier, Hermsen, & Hote 1991). Such γ-rays would be converted to $e^{\pm}$ pairs if they crossed a $B \gtrsim 2 \times 10^8$ G, and thus would not be expected to escape if produced within much less than 10 R of the stellar surface. In addition, the maximum potential drop along $\boldsymbol{B}$ which can be sustained within that distance to the star is $\sim 10^{12}$ V. At higher voltages, curvature-radiated γ-rays would produce so many $e^{\pm}$ pairs as they crossed the local $B > 10^9$ G, that such pair production would quench the acelerating potential drop. The maximum possible particle flow ($\dot{N}_0$) through any accelerator along the open field-line bundle between Geminga's surface polar cap and its light cylinder is limited to

$$\dot{N}_0 < \frac{\Omega^2 B_p R^3}{ec} \sim 8 \times 10^{31} \text{ s}^{-1} , \quad (3)$$

where B_p is the dipole field component at the stellar surface. (A current larger than $e\dot{N}_0$ would itself cause a local B near the light cylinder which is larger than that from the star.) Therefore, the maximum power from an inner magnetosphere accelerator is $e\dot{N}_0 \times 10^{12}$ V $\sim 10^{32}$ ergs s^{-1}. But Geminga's γ-ray flux in the 50–5000 MeV range is $\sim 3.1 \times 10^{-9}$ ergs cm^{-2} s^{-1} (Grenier et al. 1991), corresponding to a luminosity of 2.3×10^{34} ergs s^{-1} if radiation is emitted isotropically at the estimated distance of 250 pc. Indeed, any magnetosphere accelerator which manages to mobilize a large fraction of a pulsar's total spin-down power ($I\Omega\dot{\Omega} \sim 3.3 \times 10^{34}$ ergs s^{-1} for Geminga) must be very far from that pulsar's surface unless the pulsar is near its radio death line (Ruderman & Sutherland 1975; Chen & Ruderman 1993). The maximum possible potential drop between the surface and the light cylinder of Geminga is

$$\Delta V_{max} \sim \frac{\Omega^2 B_p R^3}{2c^2} \sim \frac{I\Omega\dot{\Omega}}{e\dot{N}_0} \sim 2 \times 10^{14} \text{ V} , \quad (4)$$

and almost all of it must be used to account for Geminga's very large apparent L_γ. Because the apparent L_γ is so close to the theoretical maximum ($\sim I\Omega\dot{\Omega}$), it is likely that there is a favorable beaming geometry which enhances the flux in our direction.

The "outer gap" accelerator model was proposed to explain needed pair production and associated energetic photon emission in the outer magnetospheres of the Crab and Vela pulsars. Such models may have application to all of the γ-ray pulsars. A turn-off for strong γ-ray emission from a Vela-like pulsar was predicted at a period $P \sim 0.13$ s by Ruderman & Cheng (1988). This period depended upon the characteristic magnetic field

through the accelerator which extends along the closed field-line boundary from the "null surface" where $\boldsymbol{\Omega} \cdot \boldsymbol{B} = 0$ out to the light cylinder. For an aligned pulsar, the outer end of the accelerator is at $r_{max} = r_{lc} = c/\Omega$. The inner end is at $r_{min} = (2/3)r_{lc}$, but it moves in sharply with increasing angle between the stellar dipole moment $\boldsymbol{\mu}$ and the spin $\boldsymbol{\Omega}$ until $r_{min} \sim (4/9)(\boldsymbol{\mu} \cdot \boldsymbol{\Omega})^2 |\boldsymbol{\mu} \times \boldsymbol{\Omega}|^{-2} r_{lc}$. The turn-off period $P \sim 0.13$ s comes from taking the characteristic B in the accelerator as that at r_{lc}. Chen & Ruderman (1993) used B evaluated at $r = 0.5r_{lc}$ which gives a γ-ray death line defined by $5 \log B_p - 12 \log P = 69.5$. Geminga, with $B_p = 1.6 \times 10^{12}$ G, falls just below this line, i.e, just beyond turn-off. However, because a substantial inclination angle between $\boldsymbol{\mu}$ and $\boldsymbol{\Omega}$ moves the inner end of the accelerator nearer to the star, it increases the accelerator's magnetic field. This could account for Geminga being a strong γ-ray pulsar rather than a moribund one. Indeed, if Vela's inclination angle, $\theta = \cos^{-1}(\hat{\mu} \cdot \hat{\Omega})$, is $\sim 35°$, and if Geminga's is $\sim 65°$, then their "outer gap" accelerators could have similar local magnetic field, size, current flow and total power (Ruderman et al. 1993). Geminga's accelerator would, however, have to span almost all of that star's accessible open field lines to accomplish this, compared to less than 1/3 of the open field lines for Vela's. With this modified inclination angle, an outer gap model which worked for Vela would probably also be applicable to Geminga. Reports of the death of such models (Bertsch et al. 1992) seem exaggerated, or at least premature.

5.2. *Beam Geometry*

Certain features of a Geminga-like outer magnetosphere accelerator seem robust enough to survive in any model of an accelerator and γ-ray emission in that region. To motivate these we shall, however, use the description of an outer-gap, Vela-like accelerator (Cheng, Ho, & Ruderman 1986a).

1. The accelerator, to avoid self-quenching by its own $e^{\pm}$ pair production, is bounded by the last closed field-line surface of Figure 8. There is a similar accelerator on either side of the star.

2. Electrons and positron accelerated through the accelerator are radiation-reaction limited, so that each accelerator is almost 100% efficient as a γ-ray emitter.

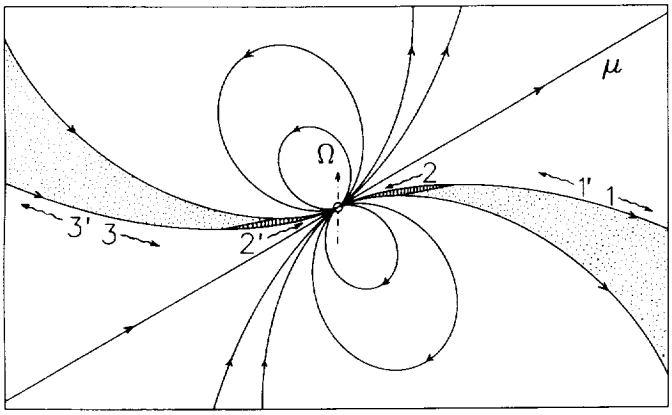

FIG. 8.—Proposed geometry of the outer magnetosphere of Geminga, showing the accelerators and γ-ray beams powered by them. The accelerator, which is relatively empty of charge, is the stippled region. The accelerator on the right (left) is bounded from below (above) by the last closed field-line surface. The open field-line bundle between the accelerator and the polar cap (*vertically shaded region*) contains $\dot{N}$, the $e^-(e^+)$ flow out of the accelerator down toward the polar cap (see also Fig. 9).

3. To achieve the high $L_\gamma/I\Omega\dot{\Omega}$ of Geminga, almost all of the appropriately curved open field lines which pass through the $\boldsymbol{\Omega} \cdot \boldsymbol{B} = 0$ surface also pass through the outer-magnetosphere accelerator.

4. Because of $e^{\pm}$ pair production within the accelerators, each produces a particle flux $\dot{N}$ of $e^-(e^+)$ moving down toward the star's polar cap from its inner end, and an equal flux of $e^+(e^-)$ moving outward from its light cylinder. In addition, there is a comparable flux of positively (negatively) charged particles pulled up from the polar caps which also passes through the accelerator. The total (maximum) flux of $e^-(e^+)$ directed down toward the polar caps is

$$\dot{N} \sim 2\left(\frac{\Omega B}{2\pi e}\right)\left(\frac{\pi}{2}\frac{R}{r_{lc}}\right)R^2 \sim 4 \times 10^{31}\ \mathrm{s}^{-1}\ . \tag{5}$$

These $e^-(e^+)$ will emit the curvature radiation beams 2 and 2′ of Figure 8.

5. Within the accelerator, pair-produced e^- and e^+ flow in both directions so that the similar fan beams of radiation, beams 1 and 1′ from one accelerator, will be matched by beams 3 and 3′ from the other. Because of Geminga's large tilt angle θ, the curvature radiation beam 2 will only be seen by observers looking within an angle greater than θ of the pulsar spin axis. It is less clear over how large an angle the fan beams 1 and 3 would be observable.

6. An observer could, in principle, see the three beams 1, 2, and 3 (or 1′, 2′, and 3′). Because of Geminga's large tilt angle, the emission radius $r_e \ll r_{lc}$ and time of flight and aberration differences among the three beams are small. The phase separation between beams 1 and 2 is $\Delta\phi = 0.5 + \delta$ with $\delta \sim 2r_e/\pi r_{lc}$. Beams 1 and 3 will merge with separation δ. Geminga's observed $\Delta\phi$ and the widths of its two pulses require $r_e < 0.05r_{lc} = 5 \times 10^7$ cm. This would imply an inclination angle for Geminga greater than 70°.

7. Because of this large angle, beams 2 and 2′, and even 1′ and 3, may come close enough to the strong inner magnetic field of the star to give a very substantial $e^{\pm}$ pair production there.

5.3. *Polar Cap Heating*

The extreme relativistic particles from the starward end of the accelerator will curvature radiate away much of their energy before reaching the stellar polar caps. Their instantaneous rate of such energy loss is

$$\dot{E} = \dot{\gamma}mc^2 = -\left(\frac{2c}{3}\right)\left(\frac{e}{r_c}\right)^2\gamma^4\ , \tag{6}$$

where $r_c \simeq (rc/\Omega)^{1/2}$ is the local radius of curvature of the (dipole) field lines which link the accelerator to the star's polar cap. For an accelerator which begins at the radius $r_{min} \gg R$, the residual energy of the $e^{\pm}$ impacting the polar cap can be approximated as

$$E(R) = \left[\frac{2e^2\Omega}{mc^2}\ln\left(\frac{r_{min}}{R}\right)\right]^{-1/3} mc^2 \sim 6.5\ \mathrm{ergs}\ , \tag{7}$$

as long as $E(r_{min}) \gg E(R)$. Then from equation (5), and choosing $r_{min} \sim r_e \sim 5 \times 10^7$ cm, the power brought down to the polar cap by particles coming from the inner ends of the outer-magnetosphere accelerator is $L_p \sim 2.6 \times 10^{32}$ ergs s^{-1}. This predicted polar-cap luminosity is insensitive to the geometry, location, or pair-production mechanisms in the accelerator,

but it does assume that the accelerator current (and power) are near maximal.

If the two heated half polar caps could be directly observed, they would have a temperature of $\sim 6 \times 10^6$ K. This is about twice the observed temperature $T_2 = (3 \pm 1) \times 10^6$ K of the hotter blackbody component. Moreover, the theoretical polar-cap heating exceeds the "hard" X-ray luminosity by a factor of 10^2 and is even a few times larger than the estimated total X-ray emission (see Table 4). While relatively small changes in Geminga's parameters (e.g., increasing the distance by a factor of 2) could accommodate an X-ray luminosity of $\sim 2 \times 10^{32}$, how the polar cap radiation is degraded in temperature by a factor of 10 remains a problem. Moreover, the observed X-rays seem to be radiated at 5×10^5 K from almost the entire neutron star surface area of 10^{13} cm^2, instead of from the 10^9 cm^2 polar cap.

One possible cause for this discrepancy arises in the large density of $e^{\pm}$ pairs near the neutron star. Their effectiveness in reflecting keV X-rays from a hot polar cap is enormously increased whenever their cyclotron resonance frequency in the strong local magnetic field matches the frequency of incident X-rays. We consider next some aspects of this problem.

5.4. *Circumstellar X-Ray Scattering*

In the geometry of Figures 8 and 9, the radiation beams 2 and 2′ can pass relatively close to the neutron star before leaving the magnetosphere. (This may also be true for beams 3 and 1′.) A 10 GeV γ-ray would be converted into an $e^{\pm}$ pair by Geminga's magnetic field if it came within 3×10^7 cm of the star; a 100 MeV γ-ray would convert if it approached within 6×10^6 cm $\simeq 6\,R$. The $e^{\pm}$ pairs materialized from the γ-rays of energy E_γ would themselves radiate γ-rays with energy $E_\gamma^{(2)} \sim 10(E_\gamma/\mathrm{GeV})$ MeV. This second generation of γ-rays could in turn also make pairs if some passed within a radius $r \sim R(E_\gamma^{(2)}/\mathrm{MeV})^{1/3}$ of the star. The pair flux thus generated increases with larger inclination angles between $\boldsymbol{\mu}$ and $\boldsymbol{\Omega}$, and might exceed 10^{38} s^{-1} for Geminga. These $e^{\pm}$ pairs are created mainly on closed field lines and will, therefore, ultimately be channeled into the near magnetosphere of the neutron star. Their abundance there depends upon the detailed location of the annihilation process, e.g., to what extent polar-cap X-ray emission and cyclotron resonant $e^{\pm}$ scattering of these X-rays keep these pairs from flowing easily down onto the stellar surface. Local number densities $n_{\pm} > 10^{15}$ cm^{-3} and column densities in excess of 10^{21} cm^{-2} seem quite plausible for Geminga.

With only a Thomson scattering cross section σ_T, these $e^{\pm}$ would have a negligible optical depth to escaping polar-cap X-rays. However, because of the stellar magnetic field the effective X-ray $e^{\pm}$ scattering cross section can be represented as

$$\sigma = \sigma_T(\hat{\mathscr{E}} \cdot \hat{B})^2 + \frac{2\pi^2 e^2}{mc} |\hat{\mathscr{E}} \times \hat{B}|^2 \delta(\omega_B - \omega) . \quad (8)$$

Here $\hat{\mathscr{E}}$ is the (electric field) polarization of the X-ray, and $\omega_B = eB(r)/mc$. With $\hbar\omega \simeq 0.5$ keV for Geminga's polar-cap X-rays, and $\hat{\mathscr{E}} \cdot \hat{B} = 0$,

$$\int_R^\infty \sigma\, dr = \frac{2\pi^3}{3} \left(\frac{e^2 R}{mc\omega}\right)\left(\frac{eB_p}{mc\omega}\right)^{1/3} \sim 2 \times 10^{-13}\ \mathrm{cm}^3 . \quad (9)$$

Thus an $n_{\pm} > 10^{13}$ cm^{-3} at $r \sim 3\,R$ would make an optically thick cyclotron resonant backscattering layer there. Most of the hot polar cap X-rays would then not escape before being intercepted by the star. In this way, polar cap X-ray power is transferred to the entire stellar surface from which it is reradiated at a predicted lower temperature T_1, where

$$T_1 \sim \left(\frac{\text{polar cap area}}{4\pi R^2}\right)^{1/4} T_2 = \left(\frac{\Omega R}{4c}\right) T_2 = 0.12 T_2 . \quad (10)$$

The predicted ratio T_1/T_2 is in reasonable agreement with the observed values and their errors as listed in Table 2. Of course, the cooler surface radiation will have to pass through its own cyclotron-resonant $e^{\pm}$ backscattering layer at $r \sim 6\,R$ before ultimately escaping. However, there is no significant further reduction in emitted X-ray energy even if some of this softer X-ray flux is also ultimately reabsorbed by the stellar surface, although the spectra shape of the emission can be affected.

A small fraction of the hard polar cap X-rays may pass through the resonant scattering layer at $r \sim 3\,R$ without being backscattered. These are the photons with $|\hat{\mathscr{E}} \times \hat{B}| \sim 0$. They are moving almost perpendicular to the local $\boldsymbol{B}$ with polarization along $\boldsymbol{B}$, so that any cyclotron resonances are not effective in amplifying their cross section. Thus, the hard X-ray component which passes through the cyclotron resonance backscattering layer might be almost completely linearly polarized.

5.5. *X-Ray Light Curves*

Any model which tries to explain as other than a coincidence the 180° separation of Geminga's two γ-ray peaks would need a highly inclined dipole. Then, if the stellar surface magnetic field configuration were nearly that of the canonical central dipole (two surface polar caps 180° apart, the hard ~ 1 keV polar cap radiation would be expected to show two similar peaks separated by 0.5 in phase. Rather, the data comprise a single peak, or perhaps two peaks sufficiently close together in phase to be unresolvable in data of the present quality. This suggests a sunspot-like configuration, such as that from a dipole much nearer the surface than a centrally located one. Radiation from a sunspot polar-cap configuration should appear brightest to an observer when the star is rotated by $\sim 90°$ from the phase angle at which γ-ray beam 2 is observed. (Fig. 9*a*). With the highly inclined dipole and sunspot-like geometry of Figure 9*b*, this emission direction is also near that for which some of the beam can have $|\hat{\mathscr{E}} \times \hat{B}| \sim 0$ (i.e., $\boldsymbol{B}$ perpendicular to the direction of propagation of the photon), and thus pass through the circumstellar $e^{\pm}$ cyclotron resonant scattering layer instead of being scattered back toward the star. The maximum hard X-ray intensity would then be expected at a phase interval $\Delta\phi \sim 0.25$ before or after γ-ray beam 2, depending on the sense of the stellar spin.

The most difficult place for the stellar X-rays to pass through the circumstellar $e^{\pm}$ resonance layer at $3R \lesssim r \lesssim 6R$ are the

TABLE 4

SUMMARY OF ENERGY BUDGET

Component	Luminosity (ergs s^{-1})
Spin-down power	3.3×10^{34}
γ-rays[a]	2.3×10^{34}
"Soft" X-rays[a]	5.4×10^{31}
"Hard" X-rays[a]	1.9×10^{30}

[a] Luminosity for a distance of 250 pc, in the isotropic case.

areas near the two open field-line bundles, because there $\boldsymbol{B}$ and $\boldsymbol{r}$ are nearly parallel. Any X-ray photon moving nearly radially outward would have $|\hat{\boldsymbol{\delta}} \times \hat{\boldsymbol{B}}| \sim 1$ so that the dominant resonant part of the scattering cross section in equation (8) is a maximum. This would cause a minimum in the observed X-ray intensity approximately coincident in phase with the γ-rays of beam 2 since these come to us from this same open field-line bundle direction. The indicated phases of the total X-ray minimum, hard X-ray maximum, and γ-ray beam 2 are sketched in Figure 10.

There is not yet a compelling determination of which of the two observed γ-ray beams should be identified with beam 2. However, beam 2 of Figure 8 should consist mainly of curvature radiation from $e^-(e^+)$ after they have left the accelerator. It would be expected to be less intense than the sum of beam 1, which contains similar radiation from $e^+(e^-)$ moving outward within and above the accelerator, plus beam 3 from inward moving $e^-(e^+)$ within and above the accelerator on the opposite side of the neutron star. This suggests identifying the weaker of Geminga's two γ-ray pulses (in Fig. 10) as beam 2. More compelling support would be a softer spectrum at the highest energies for the weaker pulse, as its most energetic γ-rays are converted to $e^{\pm}$ pairs when passing through the stellar magnetic field. If the second, stronger γ-ray pulse is mainly beam 3 of Figure 8, then its preceeding interpulse shoulder is also suggestive of what is expected from the effects of aberration on emission at larger radii (Cheng et al. 1986b). The model phases from Geminga's X-ray maxima and minima shown in Figure 10 are qualitatively similar to the observed ones in Figure 2.

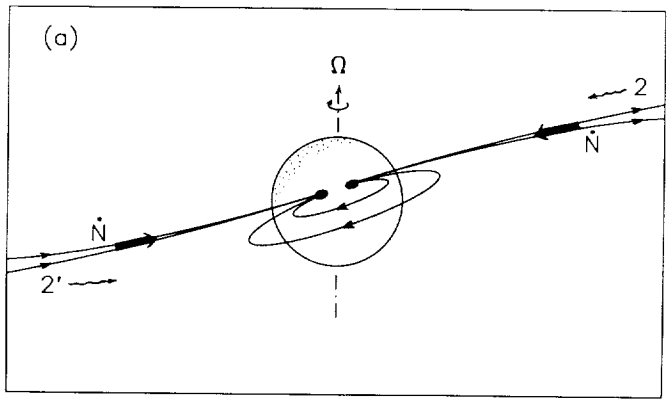

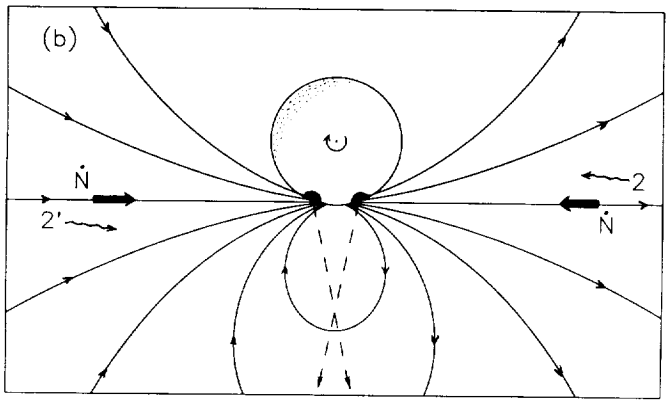

FIG. 9.—(*a*) Geometry of the surface magnetic field, showing the highly inclined sunspot dipole, and γ-ray and particle beams inwardly directed along the open field-line bundle. (*b*) Top view of the neutron star, showing the near-surface field configuration and the rotation phase for which an observer at the bottom of the figure would see the maximum hard X-ray flux. The dashed lines are the radial directions in which $|\hat{\boldsymbol{\delta}} \times \hat{\boldsymbol{B}}|$ can vanish at $r \sim 3\,R$.

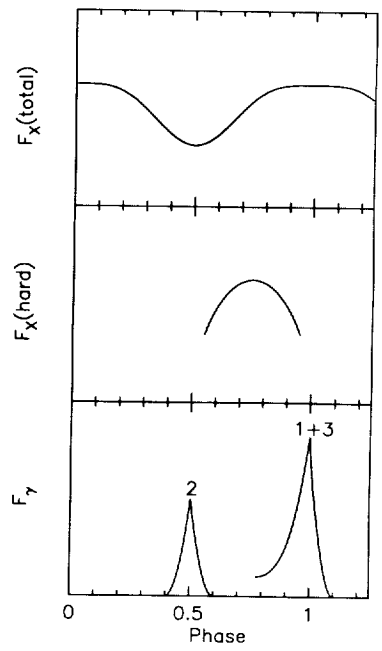

FIG. 10.—Schematic phase diagram of the γ-ray and X-ray light curves according to the theory presented in §§ 5.1–5.5. Qualitative similarities with the observational data shown in Fig. 2 are apparent.

(A comparison of the expected polar-cap heating with the observed X-ray luminosity can also be made for the Vela pulsar. Here the Ω and B are larger, but the fraction of open field lines subtended by the accelerator is probably of order 10% so that the expected polar-cap heating is $\sim 4 \times 10^{32}$ ergs s^{-1}, about the same as for Geminga. The observed X-ray luminosity in the Vela point source is 4.3×10^{32} ergs s^{-1} [Ögelman et al. 1992], which is in excellent agreement with such a model, but the inferred emitting area of 0.1 times $4\pi R^2$ is more difficult to understand: although it is much larger than the polar cap, it is still much smaller than the full surface.)

5.6. *Neutron Star Cooling Curves*

In the above interpretation, the soft X-ray component of luminosity $\sim 5.4 \times 10^{31}$ ergs s^{-1} comes from the stellar surface. Since the observed temperature of 5×10^5 K falls on the theoretical neutron star cooling curves, there may be no necessary reason to attribute the soft X-ray luminosity exclusively (or even mainly) to polar-cap heating. In view of the highly efficient conversion of the 3×10^{34} ergs s^{-1} spin-down power to radiation, it is remarkable that the soft X-rays from Geminga still fall within the range allowed by the cooling curves. The predictions of a variety of models as presented by Page & Applegate (1992) fall in the range $(1–7) \times 10^5$ for a neutron star of age 3×10^5 yr, and the Geminga data do not strongly discriminate among these. However, Page (1993) concludes that Geminga must have a superfluid core in order for its surface temperature to be compatible with most cooling

scenarios. Given the expectations for polar-cap heating, and the fact that the soft X-ray luminosity is only $\sim 10^{-3}$ of the spin-down power, the observed temperature $T_1 = (5.2 \pm 1.0) \times 10^5$ K must be regarded as only an upper limit when comparing with theoretical cooling curves. An additional reason to interpret T_1 as an upper limit is the effect of the surface magnetic field on the emergent spectrum, as discussed in the next section.

The shape of Geminga's soft X-ray pulse is very similar to that of PSR 0656+14 (Finley et al. 1992) although the statistics of the latter are poorer because the pulsed fraction is only 14%. The blackbody temperature of PSR 0656+14 is 9×10^5 K, and its characteristic age is 1.1×10^5 yr, a factor of 3 younger than Geminga. There is so far no evidence for γ-ray emission from PSR 0656+14 ($d \sim 500$ pc), or for an additional hard X-ray component. These facts together are consistent with the interpretation of the soft X-ray spectrum in both of these stars as "normal" photospheric emission.

5.7. *Magnetized Neutron Star Atmospheres*

The X-ray spectrum emergent from a realistic neutron star atmosphere can deviate substantially from a blackbody because of the nongray opacity (Romani 1987). The observed spectrum is generally harder than a blackbody at the given effective temperature. The surface magnetic field ameliorates this effect to some extent, but also introduces rotational modulation because the radiative opacity and heat conduction are anisotropic (Miller 1992; Shibanov et al. 1992, 1993; Ventura et al. 1993). These authors have modeled both fully ionized and partially ionized atmospheres, and the deviations are more substantial for the latter with light element composition, since the K-edges of hydrogen and helium are shifted into the *ROSAT* bandpass for typical surface magnetic fields. Although a detailed fitting of these models is beyond the scope of this paper, a first-order concern is whether or not magnetic effects can account for the complex spectral and pulse behavior in terms of a *single* component spectrum, without the need for two distinct blackbodies as invoked in § 3. The light-element models are the most relevant in this regard.

Beginning with a fully ionized hydrogen photosphere, Shivanov et al. (1992) showed that two models with effective temperature 5×10^5 K and $B = 4.7 \times 10^{12}$ G can differ by as much as 45% in flux at 1 keV, according to whether the magnetic field is normal or tangential to the surface. At lower energies the difference is less, and below 0.25 keV the spectra cross over. Although this anisotropy could in principle be responsible for some of the rotational modulation, it seems unlikely to be able to explain the *existence* of the hard pulse as a tail of the soft blackbody, since the observed flux at 1 keV is at least 100 times larger than the extrapolation of the soft blackbody component (Fig. 3).

The inclusion of bound-free opacity causes sharper deviations from a blackbody (Miller 1992; Shibanov et al. 1993). The theoretical spectrum closely follows a blackbody below the photoionization threshold of hydrogen, which is at ~ 200 eV for $B \sim 2 \times 10^{12}$ G. Deviations can be substantial above this energy. In particular, the spectra fall below the blackbody between 0.2 and 0.6 keV, but rise to as high as 10 times the blackbody flux at 1 keV. Miller (1992) presented models only for $T = 1 \times 10^6$ K, but it is likely that the deviations would be even larger at lower temperatures. It is not clear whether the observed X-ray spectrum and pulse behavior can be explained by these models, and it appears that only the hydrogen atmosphere is a candidate since all the heavier element atmospheres produce large flux deficits around 1 keV (Miller 1992). Although a two-component model may remain a necessity, it would nevertheless be very useful to investigate the effects of more realistic model atmospheres on the parameters derived from the soft X-ray spectrum.

5.8. *Absence of Radio Emission*

Geminga has not been detected as a radio source. Models for its 180° double-pulsed γ-ray emission suggest that it has a much more inclined dipole than most canonical radio pulsars, together with a favorably inclined line of sight to the observer. With such a geometry, it is difficult to see why Geminga's radio beams should be missed by observers who can see its γ-rays. A *radio-quiet* Geminga may, on the other hand, be just what is expected for such a neutron star. Radio emission is generally thought to be powered by an inner-magnetosphere accelerator, perhaps even one which forms just above the polar caps where the star cannot supply the Goldreich-Julian charge density, $\rho = \boldsymbol{\Omega} \cdot \boldsymbol{B}/2\pi c$, needed to maintain $\boldsymbol{E} \cdot \hat{\boldsymbol{B}} = 0$. Near Geminga's surface, this requires a charge density $n \sim 5 \times 10^{11}$ cm^{-3} and a possible flux $cn \sim 1.4 \times 10^{22}$ cm^{-2} s^{-1}. If much more charge and $e^{\pm}$ flow than this is introduced into the accelerator region, they will quench that accelerator's $\boldsymbol{E} \cdot \hat{\boldsymbol{B}}$ and, presumably, the radio emission which it supports.

Geminga appears to be an exceptionally good candidate for a pulsar in which γ-ray emission from an outer-magnetosphere accelerator produces enough $e^{\pm}$ pairs in the inner magnetosphere to quench a radio-emission accelerator which would otherwise form there. This could be accomplished by the $e^{\pm}$ pair production discussed in § 5.4. Intense γ-ray beams, e.g., beams 2 and 2′ of Figure 9, also make pairs on the upward curving open field lines on which inner-magnetosphere accelerators are expected. A large fraction of these pairs flow in toward the star and through any near polar-cap accelerator. That accelerator would be quenched if the inward flowing $e^{\pm}$ production rate is $\dot{N}_{\pm} \gtrsim 4\pi R^2 cn(R) \sim 2 \times 10^{35}$ s^{-1}. A rate exceeding this is quite plausible for Geminga because of the large intensity of its inward-directed γ-ray beams (e.g., beams 2 and 2′ of Fig. 9). For this radio-suppressing mechanism to be effective, both a high efficiency for converting spin-down power into γ-rays, and a large inclination so that a significant fraction of these γ-rays pass close enough to the star to be converted into $e^{\pm}$ pairs, are needed.

6. UNIDENTIFIED GALACTIC γ-RAY SOURCES

Two recent developments in our understanding of the population of high-energy γ-ray sources motivate a reevaluation of the likelihood that isolated pulsars can account for the majority of the still unidentified *COS B* sources in the Galactic plane. The first is the discovery that Geminga and PSR 1706−44 (Thompson et al. 1992), which are older and spin less rapidly than the Vela pulsar, also have higher γ-ray efficiencies. The efficiency of PSR 1706−44 is 7% assuming isotropic emission, and it was argued here that Geminga's efficiency is close to unity. The second development is the reanalysis of the *COS B* catalog by Mayer-Hasselwander & Simpson (1990) which, by using a better diffuse background model, leaves fewer still unidentified strong sources and a large scale height distribution for them. The high efficiencies which are possible for the older pulsars tend to expand the pool of potential γ-ray

sources, and the larger scale height decreases the distance and hence the luminosity at which they should be detected.

The number of "confirmed" *COS B* sources above a threshold of $\sim 3 \times 10^{-10}$ ergs cm^{-2} s^{-1} is only eight. The average height above the Galactic plane for these is 2°.7, which is roughly twice that of the 24 sources in the 2CG catalog (Swanenburg et al. 1981). Many of the former "sources" closest to the plane were in reality enhancements in the diffuse flux. But 10 new sources were suggested by the reanalysis. These have lower fluxes, and an even larger scale height of $\sim 6°$. Presumably the better background model enables fainter sources to be found only slightly away from the plane, so that their latitude distribution probably overestimates the true scale height of the Galactic γ-rays source population. If a population of young pulsars is to account for the *COS B* sources, they should have a scale height of ~ 80 pc, reflecting the location of their birth in a young stellar population. Adopting a scale height of 3° implies a typical distance of 1.5 kpc, rather than the 2–7 kpc originally assumed by Swanenburg et al. (1981).

The number of potential sources with flux greater than $F_{\rm min} \sim 3 \times 10^{-10}$ ergs cm^{-2} s^{-1} can be estimated from the birth rate of pulsars in the solar neighborhood, $\sim 2.2 \times 10^{-5}$ yr^{-1} kpc^{-2} (Lyne & Smith 1990). If the apparent γ-ray luminosity is a fraction η of the spindown power, then $L_\gamma = 4 \times 10^{31} \eta B_{12}^2 P^{-4}$ ergs s^{-1}, where B_{12} is the surface field in units of 10^{12} G. (Any increase in apparent luminosity due to beaming is considered here to be included in η.) The characteristic age of a pulsar is $\tau = 1.6 \times 10^7 P^2 B_{12}^{-2}$ yr, so the maximum distance to which a pulsar of age τ could be detected is $r_{\rm max} = (L_\gamma / 4\pi F_{\rm min})^{1/2} = 5.3 \eta^{1/2} (B_{12} \tau_5)^{-1}$ kpc, where τ_5 is the age in units of 10^5 yr. The efficiency η is very likely a function of age, as indicated by the trend among the four known γ-ray pulsars. A typical value for η of 0.1 will first be examined, and then a parameterization of the form $\eta = 0.2\tau_5$ will be used.

Since pulsars younger than age τ_5 would be detectable at the distance $r_{\rm max}$, the surface density of *detectable* pulsars at a distance r is $\sigma(r) = 2.2\tau_5 \beta = 11.6 \eta^{1/2} \beta (B_{12} r)^{-1}$ kpc^{-2}, where β is the fraction of γ-ray pulsars whose beaming allows detection by us. For the case of constant η, the total number of detectable pulsars to a distance D is then

$$N = \int_0^D 2\pi r \, dr \, \sigma(r) = 73 \frac{\eta^{1/2} \beta}{B_{12}} D \, , \qquad (11)$$

where D is in kiloparsecs. A typical value of D can be the distance at which the flux of a Vela-like pulsar would equal $F_{\rm min}$, or ~ 3 kpc. For $\eta \beta^2 \sim 0.1$ and $B_{12} \sim 3$, we find $N \sim 23$, which can account for the *COS B* sources.

For a model in which $\eta = 0.2\tau_5$, the maximum distance to which a pulsar is detected can be written as $r_{\rm max} = 2.4 B_{12}^{-1} \tau_5^{-1/2}$ kpc, and the surface density of detectable pulsars at a distance r is $\sigma(r) = 12 (B_{12} r)^{-2} \beta$ kpc^{-2}. The total number of detectable pulsars is then

$$N = \int_{D_{\rm min}}^{D_{\rm max}} 2\pi r \, dr \, \sigma(r) = \frac{76\beta}{B_{12}^2} \ln \left(\frac{D_{\rm max}}{D_{\rm min}} \right) \qquad (12)$$

Choosing $B_{12} \sim 3$, $\beta = 1$, and $D_{\rm max}/D_{\rm min} \sim 15$ to represent the expected range of distance between the nearest source (Geminga) and the furthest, we find $N \sim 23$ as before.

These rough calculations show that if γ-ray efficiencies of pulsars in the period range 0.1–0.24 s are typical of the ones so far detected, then the standard pulsar birth rate can account for the γ-ray source population. This birth rate assumes a beaming factor of 5 for the *radio* emission. The estimates for η used in the calculation of the detectability of the γ-rays do not assume any correlation between radio and γ-ray beaming patterns, and thus do not require the *COS B* sources to be known radio pulsars. But should we worry that the detected γ-ray pulsars might have exceptionally high γ-ray efficiencies that are *atypical* of their contemporaries? Although this is a concern, there seems to be no strong evidence that it is the case. Pulsars of the age of PSR 1706−44 or younger (17,000 yr) should be distributed with a mean separation of 1.6 kpc. Its actual distance from us of 1.4 kpc is in line with this expectation. Similarly, pulsars which are younger than Geminga (340,000 yr) have a mean separation of ~ 370 pc. The estimated distance to Geminga of 250 pc is, therefore, also typical. Vela itself, at a distance of 500 pc, is closer by a factor of 4 than the mean separation of 11,000 year old pulsars. So the evidence is that the detected γ-ray pulsars are *not* overachievers, but are rather typical representatives of their age groups.

7. COMMENTS

The *ROSAT* X-ray observation of Geminga can be interpreted in terms of thermal emission from the surface of the neutron star. A combination of constraints based on fits to the X-ray spectrum, the brightness of the optical counterpart, and the local interstellar hydrogen column can be used to restrict the likely distance to the range 150–400 pc. The surface temperature is $T_1 = (5.2 \pm 1.0) \times 10^5$ K, which is in the range of model cooling curves for a neutron star of age 3×10^5 yr. The bolometric soft X-ray luminosity is $5.4 \times 10^{31} (d/250 \text{ pc})^2$ ergs s^{-1}, but could be in error by a factor of 2 because of the effect of the uncertainty in $N_{\rm H}$ on the X-ray spectral fits.

The implied efficiency for converting spindown power into γ-ray luminosity is then greater than 25%, and a substantial beaming factor could be required as well if the upper range of the distance estimate applies. Rather than all γ-ray pulsars having efficiencies comparable to Vela ($\eta \sim 1.4\%$), the observations of both PSR 1706−44 ($\eta \sim 7\%$) and Geminga strongly suggest that the efficiency is a rapidly increasing function of period. The effect of this trend is to boost the likelihood that most of the high-energy γ-ray sources in the Galaxy are pulsars with periods in the range 0.1–0.24 s. They are not necessarily known radio pulsars, both because γ-ray fan beams can be more widely visible than narrow radio beams, and because efficient inclined γ-ray pulsars may quench their radio emission accelerators (§ 5.8).

A highly inclined rotator is favored in order to account for the large γ-ray efficiency and the 180° separation of the γ-ray pulses. Since the γ-ray efficiency of Geminga is close to unity, it is of particular interest to ask how much additional luminosity might be hidden in the energy band between the 1 keV X-rays and the 100 MeV γ-rays. A power law connecting the detections at these energies would contain only $\sim 24\%$ of the *COS B* luminosity, and would fall below the detection thresholds of all existing instruments. The claimed 2.8 σ detection of pulsed emission from Geminga by the Figaro experiment (Massaro et al. 1993) lies above this interpolation, and amounts to a flux of 1.1×10^{-10} ergs cm^{-2} s^{-1} in the 0.15–0.48 MeV range. This is only 4% of the *COS B* flux, but, if real, it could be indicative of an energetically significant component if it extrapolates over a wider energy band. It could also contain more than 10^{38} s^{-1} of $e^{\pm}$ annihilation γ-rays which may come from the pair creation mechanisms of § 5.4.

Geminga is of great importance to the study of neutron star photospheres, since it presents the most detailed pulse profile and spectrum so far obtained that can be confidently attributed to surface emission. But the X-ray pulse shapes may be difficult to analyze quantitatively. The single-peaked nature of the soft and hard X-ray pulses and their $\sim 105^\circ$ separation suggests a *surface* magnetic field geometry which includes an off-center dipole. It is not clear how much of the high-frequency structure in the soft X-ray pulse can be understood as rotational modulation of surface field, and to what extent resonant scattering in the magnetosphere may be responsible. The interpretation of the hard X-ray component ($T_2 \sim 3 \times 10^6$ K) as polar cap emission may yet be problematic: its luminosity of 2×10^{30} ergs s^{-1} falls two orders of magnitude below the expected polar-cap heating from the magnetospheric accelerator. Models in which the polar-cap emission can be redistributed over the surface, as in § 5.4, seem to deserve detailed investigation. High-resolution spectroscopy and better signal-to-noise ratio in the harder X-rays would be a blessing (or a curse) on efforts to understand the effects of the surface magnetic field and any scattering processes on the emergent X-ray spectrum and pulse profile.

We thank Hakki Ögelman for his extensive and expert assistance with the absolute timing of the *ROSAT* data. This research was supported by NASA grants NAG 5-1606, NAG 5-2051, and NAG 5-2016. This paper is contribution No. 512 of the Columbia Astrophysics Laboratory.

REFERENCES

Bertsch, D. L., et al. 1992, Nature, 357, 306
Bignami, G. F., Caraveo, P. A., & Mereghetti, S. 1993, Nature, 361, 704
Bignami, G. F., Caraveo, P. A., & Paul, J. A. 1988, A&A, 202, L1
Brinkmann, W., & Ögelman, H. 1987, A&A, 182, 71
Chen, K., & Ruderman, M. 1993, ApJ, 402, 264
Cheng, K. S., & Helfand, D. J. 1983, ApJ, 271, 271
Cheng, K. S., Ho, C., & Ruderman, M. 1986a, ApJ, 300, 522
———. 1986b, ApJ, 300, 500
Córdova, F. A., Hjellming, R. M., Mason, K. O., & Middleditch, J. 1989, ApJ, 345, 451
Finley, J. P., Ögelman, H., & Kiziloğlu, Ü. 1992, ApJ, 394, L21
Frisch, P. C., & York, D. G. 1983, ApJ, 271, L59
Grenier, I. A., Hermsen, W., & Hote, C. 1991, Adv. Space Res., 11, (8)107
Halpern, J. P., & Holt, S. S. 1992, Nature, 357, 222
Halpern, J. P., & Tytler, D. 1988, ApJ, 330, 201
Hermsen, W., et al. 1992, IAU Circ. No. 5541
Lyne, A. G., & Smith, F. G. 1990, Pulsar Astronomy (Cambridge Univ. Press), 108
Massaro, E., et al. 1993, in Proc. Compton Symp., ed. N. Gehrels & M. Friedlander (New York: AIP), in press
Mattox, J. R., et al. 1992, IAU Circ., No. 5583
Mayer-Hasselwander, H. A., et al. 1992, IAU Circ., No. 5649
Mayer-Hasselwander, H. A., & Simpson, G. 1990, Adv. Space Res., 10, (2)89
Miller, M. C. 1992, MNRAS, 255, 129
Morrison, R., & McCammon, D. 1983, ApJ, 270, 119
Ögelman, H., Finley, J. P., & Zimmermann, H. U. 1993, Nature, 361, 136
Page, D. 1993, in Proc. 1st Symp. on Nuclear Physics in the Universe, ed. M. R. Strayer & M. W. Guidry (Bristol: Hilger), in press
Page, D., & Applegate, J. H. 1992, ApJ, 394, L17
Paresce, F. 1984, AJ, 87, 1022
Romani, R. W. 1987, ApJ, 313, 718
Ruderman, M., Chen, K., Cheng, K. S., & Halpern, J. P. 1993, in Proc. Compton Symposium, ed. N. Gehrels & M. Friedlander (New York: AIP), in press
Ruderman, M., & Cheng, K. S. 1988, ApJ, 335, 306
Ruderman, M., & Sutherland, P. G. 1975, ApJ, 196, 57
Shibanov, Yu. A., Zavlin, V. E., Pavlov, G. G., & Ventura, J. 1992, A&A, 266, 313
Shibanov, Yu. A., Zavlin, V. E., Pavlov, G. G., Ventura, J., & Potekhin, A. Yu. 1993, in Proc. Los Alamos Workshop on Isolated Pulsars, The Physics of Isolated Pulsars, ed. K. A. Van Riper, R. I. Epstein, & C. Ho (Cambridge Univ. Press), 174
Swanenburg, B. N., et al. 1981, ApJ, 242, L69
Thompson, D. J., et al. 1992, Nature, 359, 615
Ventura, J., Shibanov, Yu. A., Zavlin, V. E., & Pavlov, G. G. 1993, in Proc. Los Alamos Workshop on Isolated Pulsars, The Physics of Isolated Pulsars, ed. K. A. Van Riper, R. I. Epstein, & C. Ho (Cambridge Univ. Press), 168